MASTER'S THESIS - ACOUSTICS AND AUDIO TECHNOLOGY

PINNA RECONSTRUCTION FILTER FOR BEHIND THE EAR HEARING AIDS

Sigurd Møller van Hauen

Spring 2018

Institute of Electronic Systems
Fredrik Bajers Vej 7
DK-9220 Aalborg Ø

AALBORG UNIVERSITY
MASTER'S THESIS

Title:
Pinna Reconstruction Filter for Behind the Ear Hearing Aids.

Theme:
Sound technology for the hearing impaired in collaboration with Widex

Project Period:
Spring 2018
10th semester
30 ECTS

Project Group:
18gr1063

Participants:
Sigurd Møller van Hauen

Supervisors:
Rodrigo Ordoñez (Aalborg Universitet)
Lars Dalskov Mosgaard (Widex)

Page Numbers (including appendix): 71

Date of Completion:
June 7, 2018

Abstract:

The outer ear, the pinna, shapes the incoming sound wave, giving cues for sound source localization. The microphones of *behind the ear* type hearing aid are placed behind the ear resulting in no natural shaping of the sound by the pinna, which, in turn, robs the hearing aid users of important spatial cues.
The main focus of the thesis is investigation of the transfer function from the hearing aid microphones to the ear canal. These measurements will be the base of the pinna reconstruction transfer function (PRTF) which is to restore the pinna cues for hearing aid users. A measurement setup were made which allowed for obtaining head-related transfer functions from 611 unique sound source positions in a sphere around the four subject who participated. From these measurements pinna reconstruction filters were synthesized. The PRTFs shows a great change in their directivity patterns as a function of elevation when compares to those of a delay-and-sum beamformer. Additionally, a real-time test platform was to be developed on which hearing aid signal processing can be performed in order to evaluate localization performance of the pinna reconstruction filters and compare it to a delay-and-sum beamformer. The real-time simulation platform was tested by performing dynamic binaural synthesis.

Contents

Reading Instructions

The figures in the report are produced by the author unless a source is specified. Sources are indicated by [author,year] and can be found in the bibliography. Every figure, table, equation and listing is separately numbered continuously through every chapter. Figures can be diagrams, flowcharts or graphs. Pictures of subjects appearing in the thesis is used with their permission.

The table below shows the most used abbreviations throughout the thesis

Abbreviation	Meaning
dB SPL	dB Sound pressure level re. 20 μPa
ITD	Interaural time difference
ILD	Interaural level difference
HRTF	Head-related transfer function
HRIR	Head-related impulse response
HATS	Head and torso simulator
BTE	Behind the ear
BTE-HA	Behind the ear hearing aid
BEC	Blocked ear canal
θ	Azimuth angle in degrees (°)
φ	Elevation angle in degrees (°)
Receivers	Hearing sid speaker
PRTF	Pinna reconstruction transfer function
PRF	Pinna reconstruction filter

Preface

This report presents the work performed during my master's thesis in the period february 1$^{\text{st}}$ to june 7$^{\text{th}}$ 2018.

This part is dedicated to thank the people who has shown interest in the project and enriched the thesis with ideas, knowledge, equipment and/or participated in great discussions.

The thesis work was made possible through collaboration with the hearing aid company *Widex* who kindly supplied behind the ear hearing aids that was measured. I would like to thank Widex for participating in the thesis work and especially Lars Dalskov Mosgaard who was the main contact at Widex throughout the thesis and participated in many meetings and discussions.

Furthermore I would like to thank Flemming Christensen for his advice and provision of useful HRIR data for the pre-analysis. Thanks to Dorte Hammershøi for great inputs and sharing experience within the HRTF field. I would also thank my fellow student Poul Hoang for feedback and discussions throughout the entire project period. I also appreciate all feedback from Alvero Cabrera and for participating in some of the many meetings. Claus Vestergaard Skipper is also thanked for being a huge help in setting up the HRTF measurement setup and general laboratory advice.

Lastly I would like to thank my main supervisor Rodrigo Ordoñez for guidance and support throughout the entire masters programme but especially this thesis!

Aalborg University, June 7, 2018

Sigurd Møller van Hauen

1 | Scope

Studies have shown that the spectrum shaping by the pinna provides cues used in localization of sound source positions ([Han, 1994], [Gardner and Gardner, 1973]). The position of the *behind the ear hearing aid* (BTE-HA) microphones does not capture the natural characteristics of the sound entering the ear canal, since it lacks the influence of the pinna on the incoming sound, thus could introduce localization errors for hearing aid users.

The topic of the thesis is inspired by an idea generated by Rodrigo Ordoñez from the acoustics department at Aalborg University and Alvaro Cabrera from *UNEEG Medical*. This has lead to the collaboration between the hearing aid company Widex and Aalborg University and the work of this master thesis.

The motivation of the thesis is to investigate the effects of placing the hearing aid microphones behind the ear and explore methods which could lead to hearing aid users perceiving a more natural sound. This in turn might lead to an increase in localization performance when compared to beamformer which is implemented in most modern day hearing aids.

Implementation in real life hearing aids might not be a possibility. If a method is found that could restore the natural sound of the pinna for hearing aid users, a platform on which it could be evaluated would be needed.

2 | Spatial Perception

Being able to tell in which direction a sound source is placed is crucial for animals as well as humans in survival and social situations. This chapter is to introduce the reader for the fundamentals of sound source localization, such as bi- and monaural cues, and to explore the effects of hearing aid use in terms of localization performance.

Sound source position is given in a spherical coordinate system relative to the head. Angle in the horizontal plane is denoted azimuth (θ) and the angle with respect to the horizontal plane is the elevation (φ). Both given in degrees (°). An azimuth angle of $\theta = 0°$ and elevation angle of $\varphi = 0°$ corresponds to a sound source straight and at the same height as the ear of the listener · This notation of sound source position will be used throughout the thesis.

2.1 Binaural Cues

The strongest cues for localization is when signals from both ears are compared, known as binaural cues. Localization can also be achieved using monoaural cues but are not near as strong as binaural cues. A sound source and listener example is illustrated in figure 2.1. The sound source is placed at $\theta = -45°$ and $\varphi = 0°$. This results in an interaural time difference (ITD) where $t_{left} < t_{right}$ and interaural level difference (ILD) where $L_{left} > L_{right}$ [Moore, 2013].

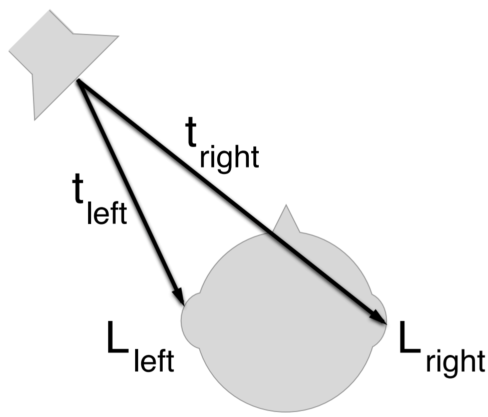

Figure 2.1: Illustration (top view) sound source and listener. Interaural time and level difference are illustrated for a sound source placed at in the horizontal plane to the left of the listener.

ITDs and ILDs has different frequency ranges where they provides their best spatial cues. At low frequencies the sound shapes around the head resulting in a lack of ILD. This phenomenon is known as diffraction. ILDs are therefore of little use below 500 Hz but can be as large as 20 dB at higher frequencies where diffraction does not play a role. This also depends slightly on the size of the head. ITD ranges from 0 μs (θ=0°) to approximately 690 μs ($\theta = 90°$ on the contralateral ear). If a pure tone is considered the ITD can be seen as a phase difference between the ears, also called interaural phase difference (IPD). The phase difference at high frequencies information produce an ambiguous clue about the placement of the sound source. For example, if a 4 *k*Hz sinusoidal tone (T=1/f=250μs) is presented at an angle leading to an ITD of 500μs, the IPD would be two complete cycles ($ITD/T \cdot 360° = 2 \cdot 360°$), hereby being an ambiguous clue for the auditory system. As mentioned before, the maximum ITD is about 690 μs leading to ambiguities beginning at $1/(2 \cdot 690\mu s) \approx 725Hz$. The ambiguities of IPD can be resolved by either moving the source relative to the head or vice versa. Despite the fact that head movements can help on the IPD issues, the upper limit is about 1.5 *k*Hz. [Moore, 2013].

The auditory system has a method to resolve ambiguities above 1.5 *k*Hz known as *phase locking*. Whenever the cochlea is stimulated, neurons in the auditory nerve will fire an impulse of electric current in the proximity of the characteristic frequency (CF). When stimulated with a pure tone the nerve firings tends to be phase locked to the waveform of the stimulus. Due to the physiology of the auditory nerves each nerve has a "recharge period" and does not fire on every cycle of the stimulus. When they do fire the interval between firings will be approximately integer multiples of the period of the stimuli. This phenomenon has an upper limit of roughly 4 to 5 *k*Hz and weak phase locking effects can occur up to $\approx$ 10 *k*Hz [Moore, 2013]. The phase locking ability therefore provides clues of the temporal pattern and are thus useful for localization.

Multiple sound sources can be placed differently yet still result in identical ITDs. The placements of these sound sources are known as "cones of confusion". Besides helping in phase ambiguities head movements can also help in resolving the cone of confusion localization error. If the head is turned 20° and the perceived change in the apparent azimuth is identical, the sound source must be in the horizontal plane. If no change is perceived the sound source must be either directly above or below the listener [Moore, 2013]. Hirsh [1971] showed that head movements improved the ability to localize sound sources.

2.2 Monaural Cues

Monaural cues are whenever a sound is presented to one ear. An example of monaural cues is the pinna effects. It is generally suggested that the pinna shapes the sound and gives important cues for localization, especially in the vertical plane [Moore, 2013]. Batteau [1967] investigated the role of the pinna by inserting microphones into the cast of human pinnae. Subjects were to judge placement of sound sources in the horizontal and vertical plane. When the cast of the pinnae were removed from the microphones, a deterioration of sound source localization were observed.

In the work by Gardner and Gardner [1973] localization experiments were also performed where a decrease in localization performance were observed in the vertical plan compared to the horizontal plane. Furthermore, occlusion of various parts of the pinna using rubber molds was investigated. When the severity of occlusion increased so did localization errors in the vertical plane. Additionally it was found that localization were better in the anterior sector compared to the posterior sector in the vertical plane.

Han [1994] investigated how the pinna encodes directional information by occlusion with acoustically absorbing material of various parts of the pinna of a KEMAR head-and-torso simulator (HATS). They concluded that the concha is the most active part if the source is at the same elevation as the ear or above. This plays a major role in localization abilities in the horizontal plane. In addition to that it was suggested that the anti helix is an acoustic amplifier for sounds coming from below.

The spectrum shaping abilities of the pinna provides important monaural localization cues. Whenever physical changes are made to the pinna a decrease in localization performance is most likely to be experienced. If a physical attribute of the pinna changes but persist one will learn to use these cues and experience normal localization performance.

2.3 Spatial Perception Using Hearing Aids

The work by Van den Bogaert et al. [2006] evaluated the localization performance of normal-hearing subject and hearing-impaired subjects fitted with commercial hearing aids in the frontal horizontal plane. It was shown that hearing aid users ability to localize was less accurate than that of the normal hearing group. It was also found that more than half the hearing impaired subjects had an increase in localization performance when tested without hearing aids. In addition to that it was found that the adaptive directional noise reduction had a negative impact on localization performance. Christensen [1999] obtained head-related impulse responses (HRIR) of 31 adults at the blocked ear canal entrance (BEC) as well as the position of behind the ear hearing aid microphone from 97 sound source positions around the subject. Impulse responses were recorded at 48 kHz and were truncated to 256 taps. The dataset will be used to analyze the gain differences between the blocked ear canal entrance and microphone located behind the ear for a few chosen source positions of interest. The dataset will be used to as a preliminary analysis of the transfer function from the hearing aid microphone to the blocked ear canal. This database will be referenced as the *1999 dataset* for the remainder of the thesis.

The relative gain difference between the BEC and BTE-HA in the frequency domain is given by:

$$H(\theta, \varphi, k) = \frac{\mathrm{HRTF}_{BEC}(\theta, \varphi, k)}{\mathrm{HRTF}_{BTE}(\theta, \varphi, k)} \tag{2.1}$$

where: HRTF_{BEC} : The frequency response at the blocked ear canal

HRTF_{BTE} : The frequency response at the behind the ear hearing aid

θ : Azimuth

φ : Elevation

k : frequency bin index

Figure 2.2 illustrates the relative gain difference given by $20 \cdot log_{10}|H|$ for $\theta = 0°, 22.5°, 45°$ and $90°$ with the elevation angle is fixed at $\varphi = 0°$. Grey lines represents the individual measurement and the solid black line representing the group mean. At low frequencies, i.e. when the wavelength is not comparable to the distance between the blocked ear canal entrance and the microphone position behind the ear, the sound pressure level (SPL) should in theory not vary. Despite this fact, a variations of ± 7 dB is seen for f<1kHz. In addition to that a bump or dip is seen at frequencies from 800 Hz to 1.1 kHz which could be caused by an object with a distance of 34 cm (at 1 kHz) to the microphone. In this case this could be an effect of the shoulder.

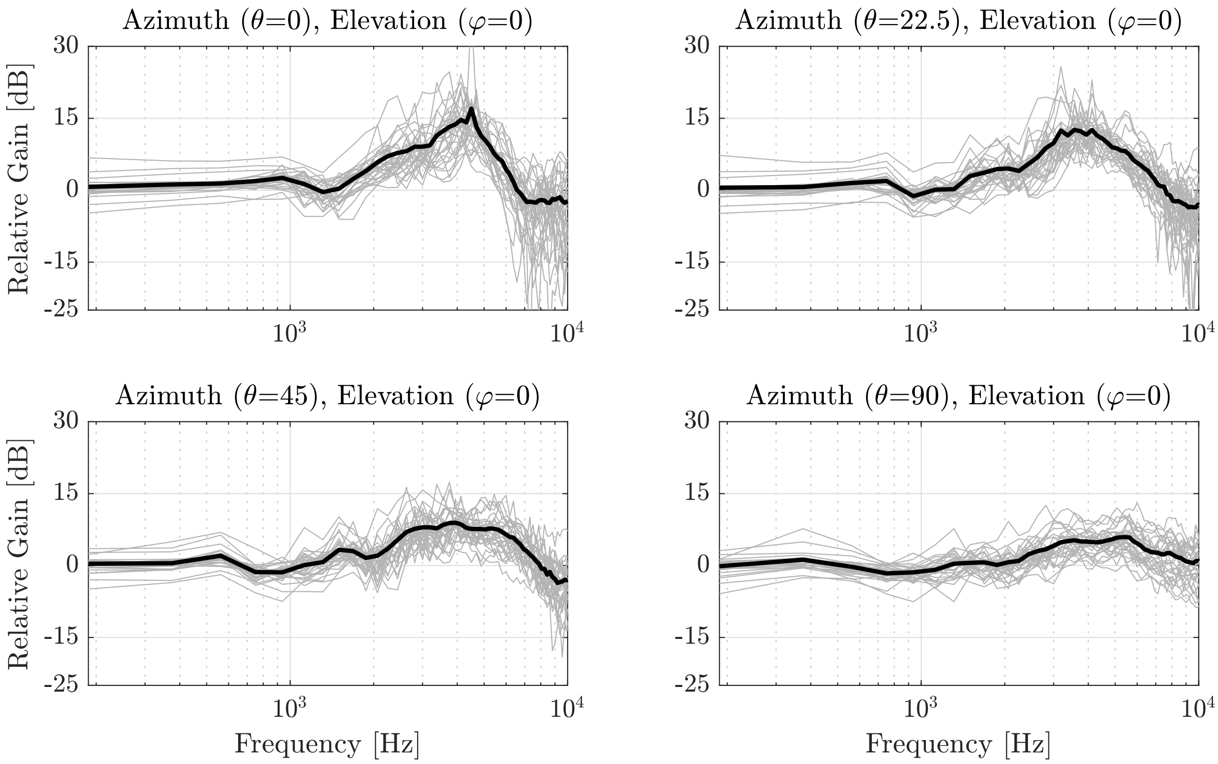

Figure 2.2: Difference in relative gain between HRTF measurement made by Christensen [1999] at the blocked ear canal entrance and at the microphone position of BTE-HA for four chosen azimuth angles. Grey lines shows individual datasets and the solid black line represents the group average.

The 1999 database has not previously been published or analyzed. Some details of the measurement procedure were orally provided by Christensen [1999]. One source of error for the low frequencies (f<1kHz) variations is believed to be measurement artifacts due to the HRIR at the ear canal entrance and behind the ear was not performed in the same measurement session. The difference is therefore most likely due to an offset in position between the measurements. Some of the subjects were elderly and were therefore seated in a chair instead of being standing. This introduces some reflections from legs and stomach, similar to those of the shoulder and torso.

The same is true for changes in measurement in the the elevation plane ($\theta = 0$), seen in figure 2.3.

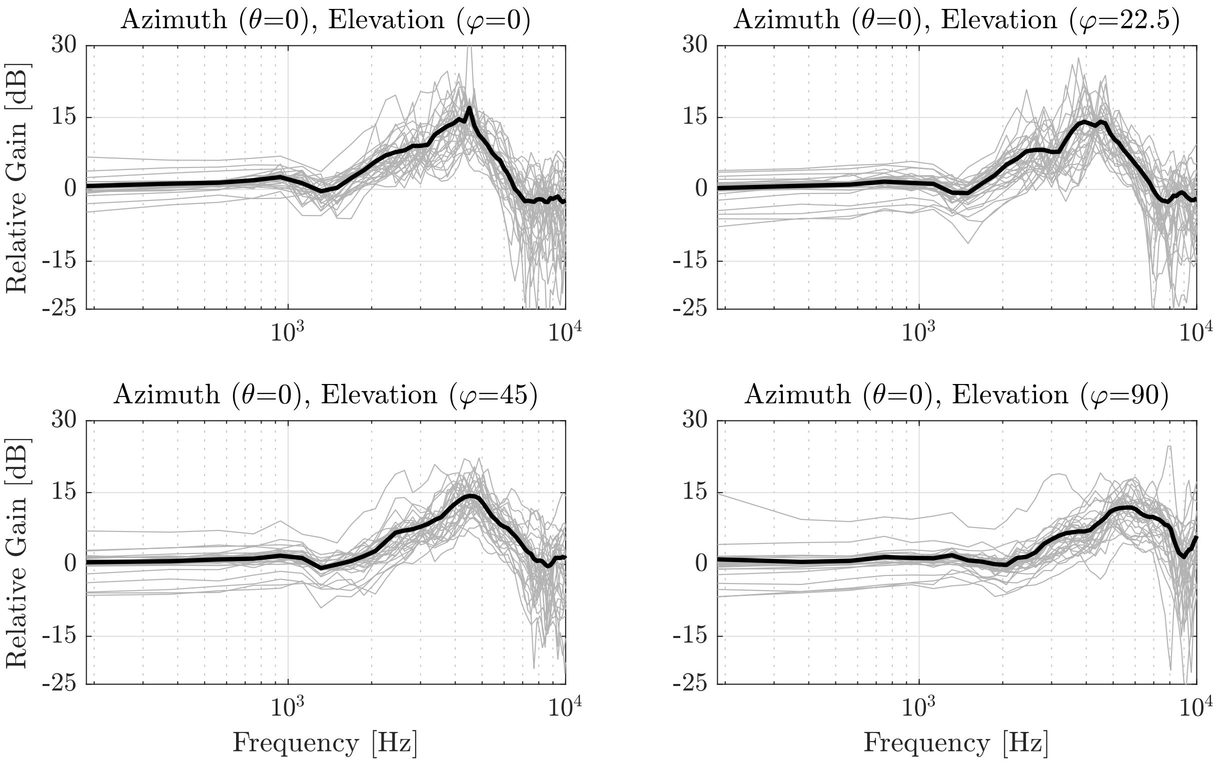

Figure 2.3: Difference in relative gain between HRTF measurement made by Christensen [1999] at the blocked ear canal entrance and at the microphone position of BTE-HA for four chosen elevation angles. Grey lines shows individual datasets and the solid black line represents the group average.

A general trend for the mean response in figure 2.2 and figure 2.3 is that the main pinna effects are seen for frequencies above 1 kHz and the pinna provides up to 30 dB gain relative to that behind the ear and is changing as a function of the sound source position.

The pinna effects contributed to the HRTF are highly individual Christensen et al. [1999] thus leading to individual pinna reconstruction transfer functions which is also seen figure 2.2 and figure 2.3.

Gardner and Gardner [1973] showed an decrease of localization abilities in the median plane when the pinnae were occluded. Combining that fact with the analysis of the 1999 dataset, it is not unreasonable to suggest that placement of the microphone behind the ear and not correcting for this could reduce hearing aid users ability to localize sound sources. This suggest that effects of the pinna is of importance in localization in most directions and an effort should be made to restore the pinna cues. This is further backed up by evidence documented by Udesen et al. [2013] which showed microphone placement behind the ear can lead to ILD changes up to 30 dB.

2.4 Aim of the Thesis

The dataset obtained by Christensen [1999], and the analysis performed in the previous section, shows that the gain difference between the microphone positions which is highly dependent on the angle of incidence. The aim of the thesis is to measure and develop pinna reconstruction filters to restore the naturalness and increase localization performance of hearing aid users.

Møller et al. [1996] showed that localization performance decreases when non-individualized binaural recordings compared to individual recordings. It has therefore been chosen to create individualized pinna transfer functions and not a generalized models based on e.g. measurements on a head-and-torso simulator.

Mueller et al. [2012] created an virtual sound environment in which hearing aid algorithms can be evaluated. Using individualized head-related transfer functions and room simulations they created convincing sound environments where localization abilities were preserved. They did however not allow for head movements which they suggest to be added using head motion sensors. This corresponds well with the work by Brimijoin et al. [2013] who showed head movements plays a significant role on being able to externalize sound sources when reproduced with headphones. An effort should therefore be put in allowing for head movements. An additional aim of the thesis is therefore to create an virtual sound environment on which localization performance of pinna reconstruction filters can be evaluated where the natural head movements show be compensated for. In order to offer a fair comparison for the hearing aids a simple beamforming algorithm will be developed and implemented.

The thesis consists of 3 main parts which corresponds to the next 3 chapters:

1. Measurements of head-related transfer functions
2. Directionality of Hearing Aids
3. Implementation of a real-time virtual sound environment platform that allows for head movements

2.5 Delimitations

The work of the thesis is not to be restricted by the current hearing aid technology or have any goals of real-life implementation in todays hearing aids. Widex provides BTE-HA "hangers" with free access to the microphones and speaker (also referenced to as "receivers"). No signal processing features of the hearing aids will be used and all signal processing develop during the thesis work will be implemented on an external processing platform such as a laptop or similar. Furthermore, some of the work in the thesis will be performed with the assumption that the sound source position is calculated and known by the hearing aid. It is not unreasonable to believe this will be a feature in future hearing aids.

3 | Head-Related Transfer Functions

Head-related transfer functions describes the filtration performed by the physical attributes of the body and external ear which is highly dependent on the angle of incidence.

The goal is to obtained HRTFs for the blocked ear canal as well as both microphones of the BTE-HA provided by Widex. The transfer function can then be found from BTE-HA microphones to the BEC in the same manner as shown for the 1999 dataset.

This chapter will describe the theory of HRTFs, the measurement setup and processing of impulse responses to HRTFs for the two BTE-HA microphones and those placed in the BEC.

3.1 Definition of Head-Related Transfer Functions

When a subject is placed in a free field scenario the person will obstruct the incoming sound wave. Here the body (head, torso, pinna etc.) cause a linear filtering of the signal. This filtration is described by the HRTF [Blauert, 2005] and is defined as:

$$\mathrm{HRTF}(\theta, \varphi, k) = \frac{P_{BEC}(\theta, \varphi, k)}{P_0(k)} \tag{3.1}$$

where: P_{BEC} : The blocked ear canal

P_0 : The Position correspond to the middle of the head in free field

The reference frequency response measurement, P_0, should be measured with the same microphone as used for measuring P_{BEC} so that both speaker and microphone response are removed in the HRTF. The reason for obtaining the frequency response at the BEC is to eliminate the ear canal resonances and can be done while still obtaining the full spatial information [Møller, 1992].

3.2 Interpolation of HRTFs

The angular resolution of the HRTFs is not strictly limited to the angles of which they are measurement as angles between measured points can be found by the means of interpolation. There are several methods of interpolating HRTFs. In the work by Minnaar et al. [2005] interpolation were performed in time domain of the neighboring HRIR in either the horizontal or vertical directions. This is advantageous as the amount of measurements can be reduced and any angle of HRTF can be found by interpolation.

Sandvad [1996] used an interpolation scheme using the four closest HRIRs in horizontal as well as vertical directions:

$$\widehat{h} = \sum_{n=1}^{4} w(n) \cdot h_n \tag{3.2}$$

where: $\widehat{h}$: The interpolated HRIR

h_n : The n^{th} closest measured HRIR

$w(n)$: weighing coefficient of the n^{th} HRIR

The weighing coefficient are given by:

$$w(n) = \frac{V(n)}{\sum\limits_{m=1}^{4} V(m)} \tag{3.3}$$

where

$$V(n) = \frac{|\theta(4) - \theta(1)| \cdot |\varphi(2) - \varphi(1)|}{|\theta(x) - \theta(n)| \cdot |\varphi(x) - \varphi(n)|} \tag{3.4}$$

where: $\theta(x)$: Target azimuth

$\varphi(x)$: Target elevation

Neighboring sound source locations are indexed as illustrated in figure 3.1.

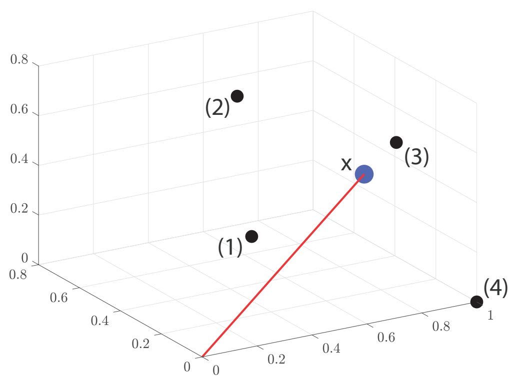

Figure 3.1: Illustration of sound source positions and numbering for interpolation. Red line represents the direct path from interpolation point to the receiver.

An example of this interpolation scheme can be seen in figure 3.2. Here a target location of $\theta = 12°$, $\varphi = 4°$ is chosen as its not included as a measured sound source location. The four closest measured sound source locations are: ($\theta = 9°$, $\varphi = 0°$), ($\theta = 9°$, $\varphi = 8°$), ($\theta = 18°$, $\varphi = 8°$) and ($\theta = 18°$, $\varphi = 0°$)

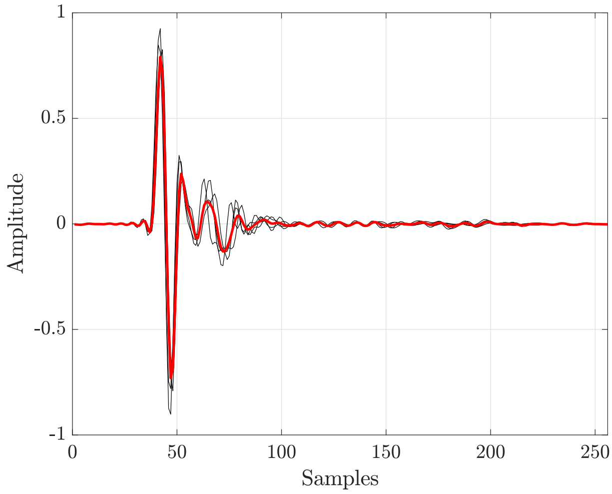

Figure 3.2: Interpolated HRIR (red line) based on the four closed measured HRIR to the target position (black lines).

3.3 Sound Source Positions

The HRTFs are required to be obtained in order to recreate a sound scenario for localization experiments using the individualized pinnae filters. As the HRTFs are to be measured on a number of individual subjects the time spent measuring the HRTFs on each subject should be minimized. Minnaar et al. [2005] showed that the number of measurement points could be reduced from 11975 points in a sphere around the head to 1130 by the means of linear interpolation without introducing errors.

Minnaar et al. [2005] found that by interpolation in the horizontal plane can be made without audible difference for HRIRs measured with angular resolution of 24° for $\varphi > 45°$. In addition, a 16° for $\theta < 45° \wedge \theta > 135°$ and 4° to 8° for the remaining directions where the side of the head in general requires most resolution. This is mirrored to angles on the left side of the subject.

Using these guidelines HRTFs need to be measured from 611 sound source positions. This is illustrated in figure 3.3a, figure 3.3b and figure 3.4.

The chosen angular resolution in azimuth of 9° was chosen for $\theta < 45°$, 5° for $45° < \theta < 135°$ and 9° for $135° < \theta < 180°$. For the elevation plane an angular resolution of 8° was chosen for $-40° < \varphi < 40°$. Measurements are made for $\theta = 0°$ and $\theta = 360°$ which is the same azimuth angle. This is done for two reasons: The first reason is that 11 measurements are duplicates and can therefore be compared in order to validate test-retest reproducibility. The second reason was due to an increased ease in the processing of the HRTFs to handle the angle "wrapping" around $\theta = 0°$ in the algorithm that finds the 4 closest measured HRTFs.

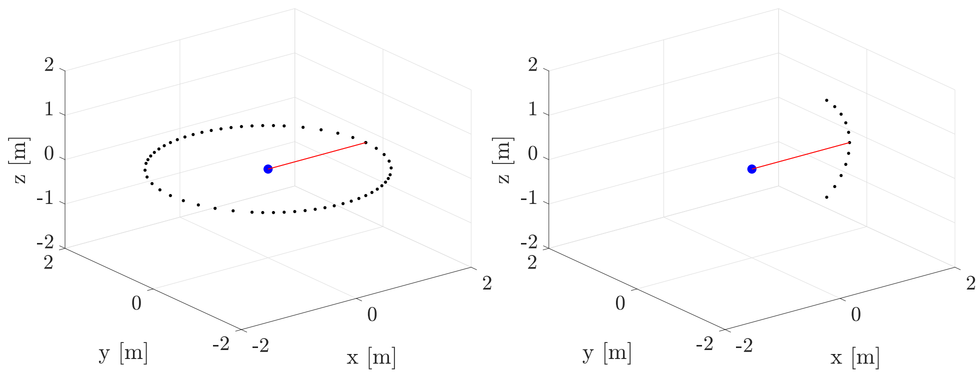

(a) Speaker positions for $\varphi = 0°$. **(b)** Speaker positions for $\theta = 0°$.

Figure 3.3: figure 3.3a illustrates the rotations in the horizontal plane chosen. figure 3.3b illustrates the speaker placement in the median plane.

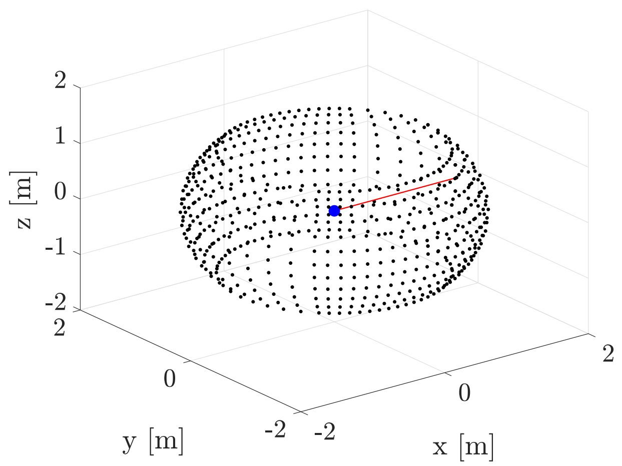

Figure 3.4: Chosen sound source positions relative to the head of the subject (blue). The red line illustrates the direction for the sound source straight ahead.

A measurement session to obtain HRTFs for all sound source positions can be measured in ≈ 30 minutes (found experimentally, see section 3.6). Additional time will be required for fitting of microphones and instructions of the subject.

3.4 Does the Shoulder Matter?

It was indicated in section 2.3 that reflections of what might be the shoulder could influence the relative gain difference between the blocked ear canal and at the BTE-HA. It was also hypothesized that the large variation at low frequency was due to the measurement procedure.

To explore this an experiment was performed in order to validate wether or not the shoulder and torso reflections matter and to test the hypothesis that simultaneous measurements will reduce the variation seen at frequencies lower than 1 kHz.

Experimental Setup

For this experiment VALDEMAR, a head-and-torso simulator designed by Christensen and Møller [2000]), was fitted with a microphone in a blocked ear canal and 3D printed BTE-HA dummy [virmary, 2018] as the Widex BTE-HA were not available at the time of the experiment. The setup are illustrated in figure 3.5a. The 3D printed hearing aid dummy and placement of the miniatuear microphone in the blocked ear canal is shown in figure 3.5b.

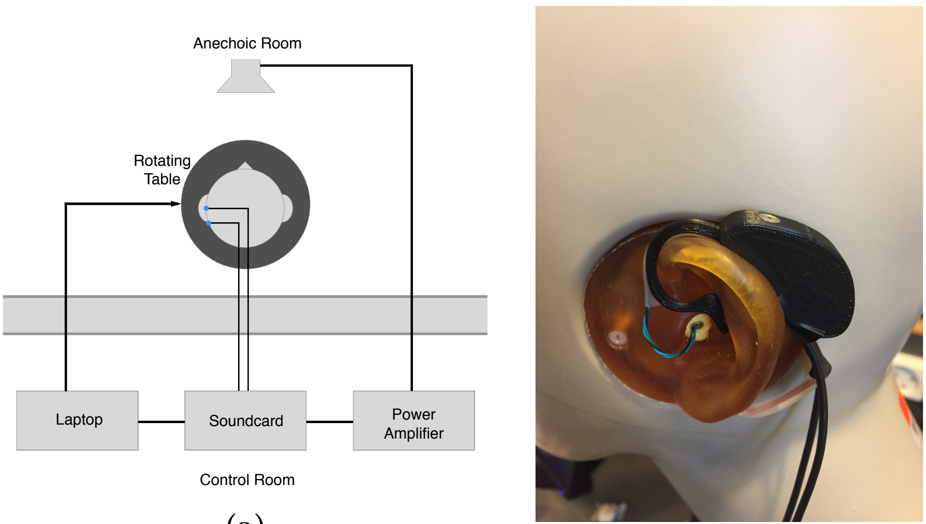

(a) (b)

Figure 3.5: On the left a schematic of the setup is shown. Right picture shows the VALDEMAR HATS fitted with a dummy BTE-HA and a miniature microphone in the blocked ear canal.

VALDEMAR is placed on the Outline 250-3D [2018] rotational table inside an anechoic room [2018]. A ball speaker is placed 1 meter from the HATS with an initial azimuth position of θ=0°. The 3D printet hearing aid dummy is fitting with the Sennheiser KE4-211-2 microphone and placed on the HATS. Furthermore, the HATS is fitting with the knowles FG-23329 microphone in the blocked ear canal using classic earplugs. Connections are made through connection-boxes to and from the adjacent control room. The Outline rotating table is interfaced via ethernet cable and an UDP connection is used for operation. An additional experiment were made where absorbent material were placed on the shoulders of the HATs. If the shoulder does matter a change should be visible when adding absorbent material to the shoulders. This was performed as the head of the HATS could not be detached from the torso.

The impulse response from speaker to both microphone poisitions were obtained using maximum-length sequence (MLS) at 1° angular resolution in azimuth at a fixed elevation of $\varphi = 0°$.

Equipment

All items for the experiment is found in table 3.1.

Item	Description	AAU-no.
1	Macbook Pro (medio 2012)	N/A
2	MATLAB 2017b	N/A
3	RME Fireface UFX II Sound card	108227
4	Pioneer A-656 Power Amplifier	08698
5	1 x Ball Speakers	2017-20
6	VALDEMAR head and torso simulator	2150-02
7	E.A.R Classic earplugs	N/A
8	Knowles FG-23329 Microphone	N/A
9	Sennheiser KE4-211-2 Microphone	N/A
10	3D printed BTE-HA dummy	N/A
11	Outline Rotational table	N/A
12	Absorbing material (cotton wool mats)	N/A

Table 3.1: Equipment used in measurements. AAU-no is an internal identification number of the equipment and is reported if available.

Results

Figure 3.6 shows a comparison of the thesis measurements to those of the 1999 dataset. Red lines show thesis measurement with added absorbing material on the shoulders [1] and blue is without this material. Black line corresponds the mean of the 31 subjects from the 1999 dataset. Error bars corresponds to ± 1 standard deviation.

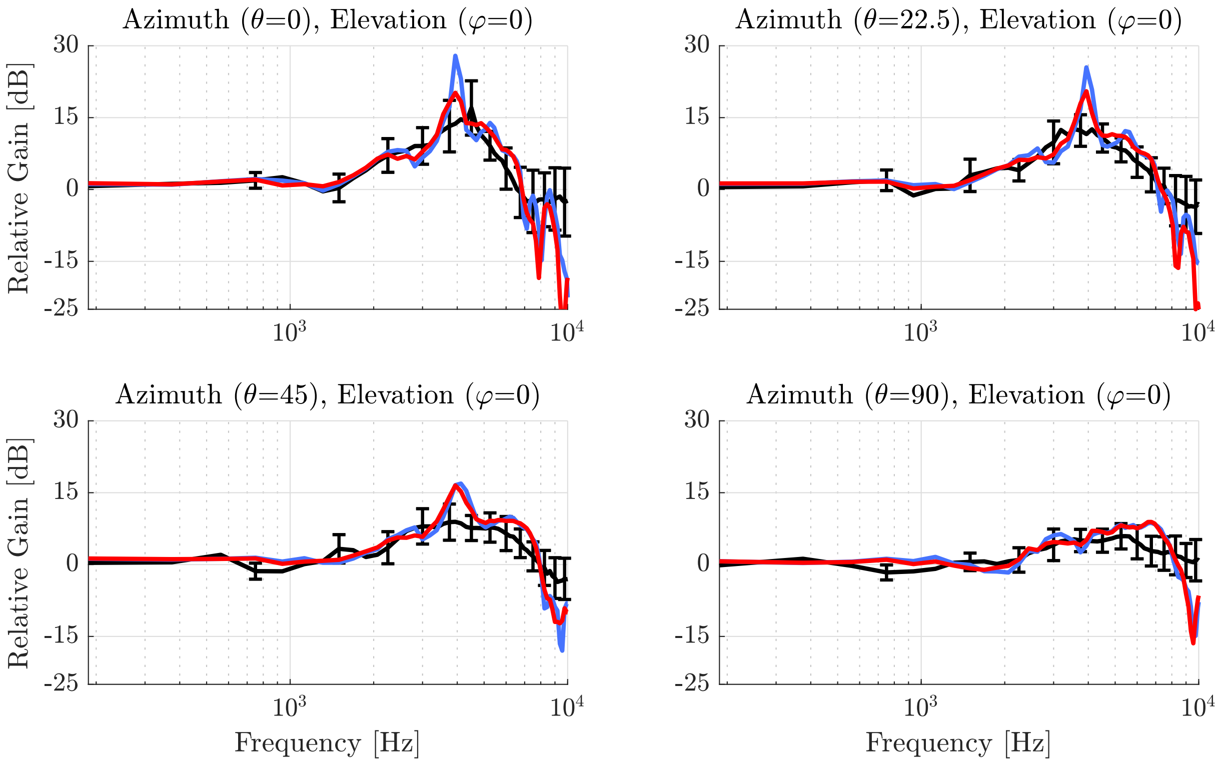

Figure 3.6: Difference in relative gain between measurement made at the blocked ear canal entrance and at the microphone position of BTE-HA as a function of change in azimuth. Black lines represents the mean response as seen in figure 2.2 with errorbars indicating ± 1 standard deviation. Blue and red lines is measurements without and with absorbent material respectively.

The thesis measurement without absorbing material on the shoulders corresponds well with the 1999 dataset for the sound source positions shown. It is important to note that the the thesis measurement is made for a single subject (VALDEMAR) unlike the 1999 dataset which is of 31 subjects. It can be seen that the standard deviation is increasing with frequency which is expected by the comb-filter structures. The single measurement aligns almost perfectly well with that of the group mean and does not reveal why deviations of ± 7 dB for f<1kHz should appear in the 1999 dataset. The experiment was repeated with absorbing material on shoulder and torso (red). Here no changes in the frequency response can be seen when compared to the measurement of no absorbing material. The deviation at the sharp peak at 4 kHz for $\theta = 0°$ and

[1] It was later realized that the cotton wool is not a good absorber at lower frequencies which is why only small changes appear at the higher frequencies. Due to time limitations of the project the experiment was not repeated using a better absorber.

$\theta = 22.5°$ is believed to be a contribution of a small position change between measurements.

Figure 3.7 shows a graphical representation of the relative gain difference as a function of azimuth. On the left the current thesis measurement at 1° angular resolution is seen and on the right the 1999 database with 22.5° resolution.

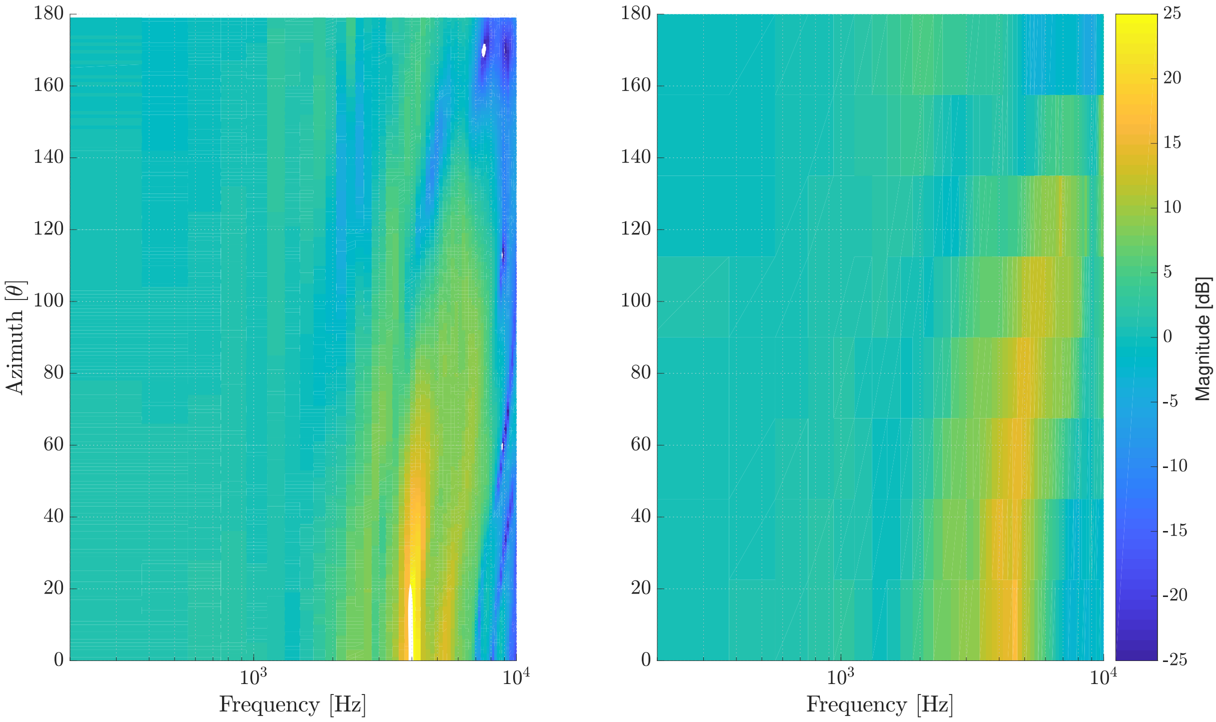

Figure 3.7: Difference in relative gain between measurement made at the blocked ear canal entrance and at the microphone position of BTE-HA as a function of change in azimuth. Left: Data from current thesis at 1° resolution, Right: Visualization of measurements made by Christensen [1999] at 22.5° resolution.

As the plot for the 1999 dataset is the result of meaning 31 individual HRIRs the relative gain pattern seems smeared out in the frequency dimension as well as as a function of azimuth thus making the fine structures less pronounced as the current measurement on one single "individual".

This validation experiment offers evidence that the shoulder does not effect the difference between the blocked ear canal and the position behind the ear as the bump/dip at 800 Hz to 1.1 kHz is far less noticeable in the thesis measurements. This narrows the frequency region of interest to be f>1kHz. It can furthermore be noticed that the gain difference is close to 0 dB for f<1kHz which reinforces the belief that the variations of the 1999 dataset in this region was due to measurements across multiple measurement sessions, and not due the shoulders.

3.5 HRTF Measurement Setup

This section is dedicated to document the physical setup used in measuring head-related transfer functions of standing adult subjects to the blocked ear canal as well as both microphones of the behind the ear hearing aids.

Design of HRTF Measurement Setup

As a physical setup using 627 speakers is impractical it is proposed to utlized the number of speakers corresponding of the number of elevation angles. Following aforementioned guidelines the elevation angles are proposed to be φ = -40° to 40° in 8° increments. When the subject is rotated along the longitudinal axis it is possible to obtain all the sound source positions as shown in figure 3.8. An Outline 250-3D [2018] turntable is utilized for this purpose due to its ability to handle the weights of an adult, can turn at a high angular resolution (0.5°) and is controllable via UDP protocol. The entire setup for HRTF measurements are located inside a large anechoic room [2018]. A diagram for the proposed setup is illustrated in figure 3.8.

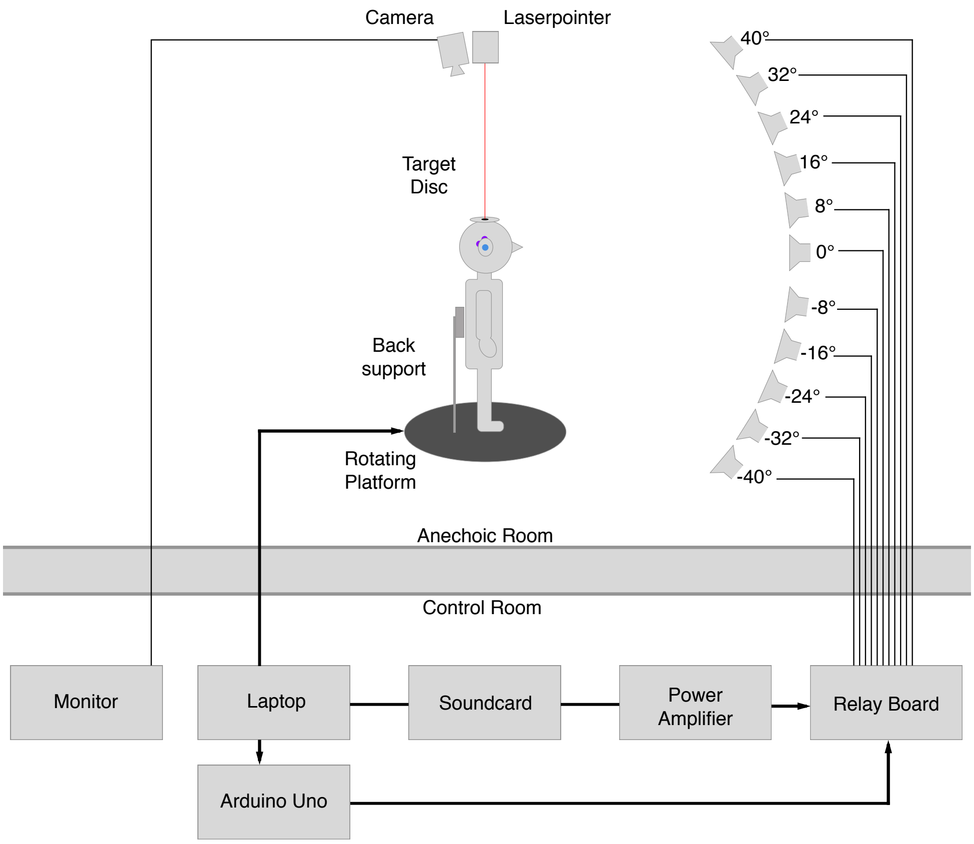

Figure 3.8: Illustration of HRTF measurement setup in anechoic conditions. Purple dots illustrates the approximate placement of the BTE-HA microphones and the blue a miniature microphone in the blocked ear canal of the subject. Connection wires to these microphones are omitted to reduce complexity of the illustration.

The mono output of the power amplifier is switched to one of the 11 speakers using an Arduino Uno and a custom made relay board. The blue circle are the microphone in the blocked ear canal and the purple circles represents the front and rear microphones of the BTE-HA. This is identical on the contralateral side of the subject. Wires from all microphones and external circuits to the the hearing aid are connected to the sound card and are not shown in the figure for simplicity.

In order to monitor the position of the head, a target disc is mounted on top of the head with a visible dot of the longitudinal axis. A laser pointer is mount directly above the subject. When turned on a red dot should be placed on the target disc throughout the measurements. The operator can monitor the movement of the subject using the camera mounted closely to the laser pointer. If the subject is moving off the target the operator can choose to pause the measurements and direct the subject to the correct position. Some back support is mounted on the rotating platform in an attempt to stabilize the subject without introducing unwanted reflections.

Widex Fusion

Widex has for the thesis work provided so-called BTE-HA "Hangers". The supplied model, *Fusion*, is depicted in figure 3.9. These hangers are "inert" hearing aids, i.e. only microphones and the speaker (also called receivers) are present hence no signal processing are performed in the hearing aids.

Figure 3.9: Product picture of the commercially available Widex Fusion [Widex, 2018]. Receiver is not depicted in this figure.

The provided BTE-HA are of the "receiver-in-the-ear" (RIC) type, meaning the small speakers, also known as receivers, are placed in the ear canal using molds of difference sizes and materials. This is opposed to the models where speakers are placed in the hearing aid housing and the acoustic signal is delivered to the ear canal using tubing.

The microphones used in the provided Widex Fusion hangers are Sonion [2018] type 8002. This information was provided by Widex. Break-out wires are added to the two microphones, front and back, and the hearing aid speaker for recording and reproduction purposes using an external sound card. Furthermore, external circuits were provided for microphone biasing using standard 1.5 Volt AAA batteries. Whenever measurements made on behind the ear hearing aids it will refer to the Widex Fusion provided by Widex unless otherwise noted.

Measurement Harness

The hearing aid microphone biasing circuitry has to be in close proximity to the hearing aids and must therefore be placed on the subject during measurements. A GoPro action camera harness was therefore used to strap the circuits to the subject which also provides stress relief on the hearing aid wires. The developed mounting harness can be seen on a subject in figure 3.10.

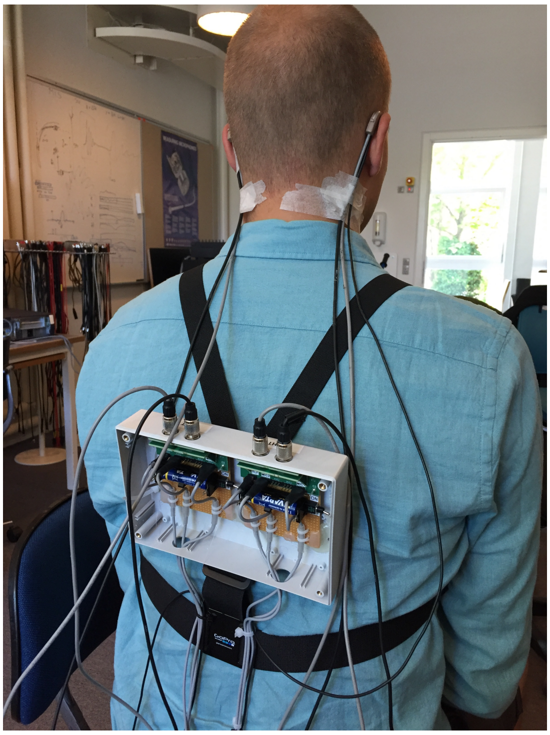

Figure 3.10: Mounted bias circuitry and microphone wires to a GoPro chest mount.

Support of the Lower Back

Standing upright and perfectly still for 30 minutes is not an easy task for the subjects as fatigue will occur within minutes. To ease this task a support for the lower back of the subject is added. Neck and/or head fixation was considered but not implemented as additional physical structures around the head could introduced unwanted reflections in the HRTFs in the frequency region of interest.

Mounting of Speakers

A metal arch bend with a radius of 1.72 meters was used as mounting points for the 11 ball speakers. Being a large physical construction, speakers and metal mounting is a source of unwanted reflections. Cotton wool mats where cut and wrapped around the entire construction, providing absorption of these higher frequency reflections. Lower frequency reflections is removed digitally by the means of windowing the measured impulse responses.

Microphone Positioning

An example of fitting of the BTE-HA and microphone in the blocked ear canal is seen in figure 3.11.

Figure 3.11: Fitting of hearing aid and microphone in the blocked ear canal on subjecting using medical tape.

A classic foam earplug was, prior to fitting, trimmed in length and a small indent burned with a soldering iron for the microphone to rest. After insertion of the earplug and microphone, the microphone wires was guided out of the ear canal and out via the intertragic notch. The BTE-HA was placed at the approximate place of normal use. In normal use the BTE-HA is supported by the receiver in the ear and the hearing aid mold. For these measurements the receiver can't be inserted due to the blocked ear canal and was therefore supported by medical tape on the breakout wires of the hearing aid.

Equipment

Equiment used for the HRTF measurement setup is listed in table 3.2.

Item	Description	AAU-no.
1	Macbook Pro (medio 2012)	N/A
2	MATLAB 2017b	N/A
3	RME Fireface UFX II Sound card	108227
4	Pioneer A-656 Power Amplifier	08698
5	11 x M10MD39-08 in ball mount	XXX
7	E.A.R Classic earplugs	N/A
8	2 x Knowles FG-23329 Microphone	N/A
9	Outline Rotational table	N/A
10	12 channel Relay Board	N/A
11	Arduino Uno	N/A
12	2 x Widex Fusion Hangers	N/A
12	GoPro Chest Mount	N/A

Table 3.2: Equipment used in HRTF measurement setup.

For the speakers Vifa M10MD-39-08 drivers are mounted in trawling net floatation balls, made by Department of Electronic Systems [2018].

Maximum Length Sequence

It has been chosen to obtain the impulse responses using maximum lengths sequence (MLS). The MLS sequence is a pseudo-random noise used as an excitation signal for the system analysis. An MLS length of 4095 was chosen as being the shortest sequence while still not introducing time aliasing. This corresponds with the method described by Møller et al. [1995]. The excitation signal is a "nasty" signal which is why the power amplifier for the speaker is set at a moderate level in order to avoid distortion. The sound pressure level at the head position was ≈ 75 dB SPL and did not introduce distortion in obtained the impulse responses. The theory of obtaining the impulse response by computing the circular cross correlation of the excitation signal with the recorded signal will not be further described in the thesis. MATLAB 2017b has an MLS implementation, (*impulseResponseMeasure*), where the core elements will be used in obtaining the impuls responses. All impulse response measurements were truncated to 256 taps which ensured all impulse responses were decayed within this time frame.

Reference Measurements

Before HRTFs can be created reference measurements has to be obtained in the position correspond to the middle of the head.

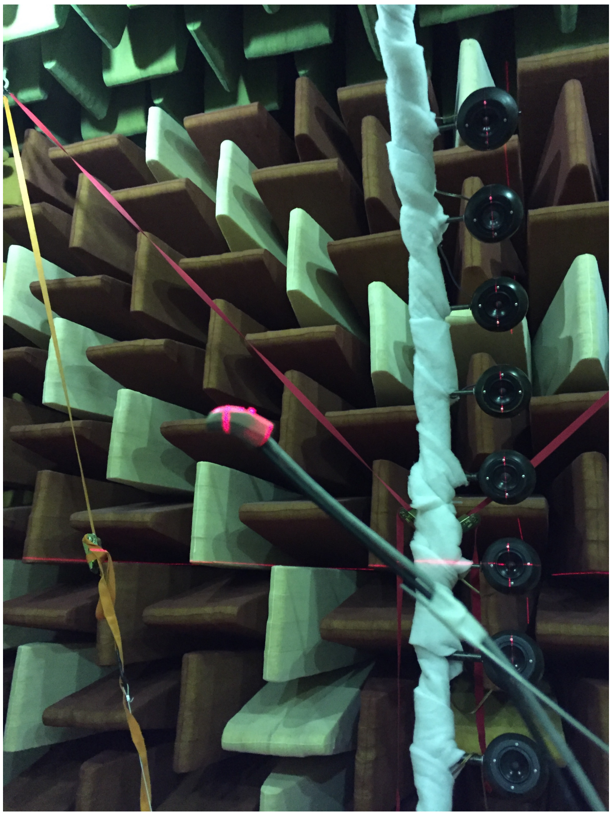

Figure 3.12: Widex Fusion hearing aid placed on a metal wire at the position of the middle of the head with the head absent. The red color on the hearing aid is caused by the guiding laser lines. The same method was utilized for the miniature microphones placed in the blocked ear canal.

Figure 3.12 shows one of the two BTE-HA placed at the position of the middle of the head with the head absent using a piece of stiff and thin metal wire which causes minimal disturbance of the sound field. The top plastic shielding was removed from the hearing aids as it is only the influence of the microphones which is desired to be deconvovled. Ideally the microphones of the hearing aid would have been completely separated from housings but was not an option during the thesis work. The hearing aid is placed with the side facing the speaker array in such a way that a phase difference will not be introduced between the two microphones of the hearing aid.

3.6 HRTF Pilot Measurements

Four male subjects participated in a pilot experiment for the HRTF measurement setup. The test subjects was fitting with a miniature microphone in the blocked ear canal and the BTE-HA were secured bilaterally with medical tape to prevent the positions to change before or during the measurements. An example of a fitting is illustrated in figure 3.13.

Figure 3.13: Pilot subject 1 fitted with microphone in the blocked ear canal and a BTE-HA.

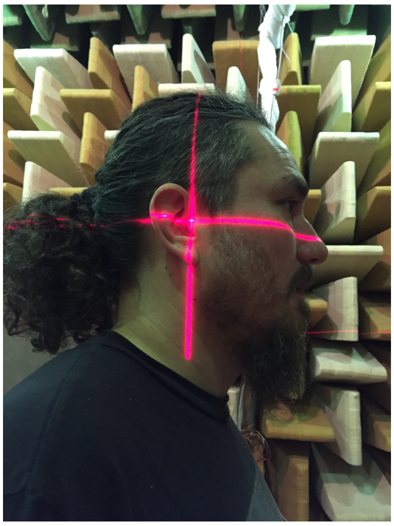

Figure 3.14: Pilot subject 1 adjusted in the measurement setup guided by lasers.

Figure 3.15: Pilot subject 1 placed in the measurement setup ready for measurements.

Two laser leveling tools were used to ensure the appropriate height and general placement of the subject. Wooden boards were placed underneath the subject to achieve the correct measurement height so that speaker 6 is at $\varphi = 0°$. This can be seen in figure 3.14 and figure 3.15. After fitting of microphones and the subject placed in the setup the measurements could begin. Total measurement time for all four pilot experiments did not exceed 28 minutes. This timeframe does not include fitting and instructions to the subject.

It was experienced that the experiment operator could not leave the subject in the anechoic room alone as the cables from the setup to the subject had to be moved and adjusted to avoid getting stuck. The top laser pointer and camera system was therefore never used. Due to this choice, the positioning of the subject were not monitored during measurements and only big movements would be re-done. Small movements due to instability, tiredness etc were therefore accepted in order to maintain a reasonable measurement time. In addition to that it was decided to give the subject 1 minute of free movement on the platform every 90° as the subjects found it hard to maintain the same exact position for 25 minutes.

3.7 Processing of HRTFs

HRTFs are to be processed for the blocked ear canal as well as both microphones of the behind the ear hearing aid. The HRTF is obtained by the complex division in the frequency domain:

$$\mathrm{HRTF}_{BEC}(\theta, \varphi, k) = \frac{P_{BEC}(\theta, \varphi, k)}{P_0(k)} \cdot H_{LP}(k) \tag{3.5}$$

where: H_{LP} : Frequency response of a low-pass filter

Sampling a signal using a sound card will include a sharp anti-aliasing filter hereby attenuating strongly near half the sampling frequency. If this is not taken into account instability in the resulting HRIR might be seen. Additionally, the type 8002 microphones from Sonion [2018], used in the hearing aid hangers, are known to roll off at 10 *k*Hz. A low-pass filter is therefore designed to have a cut-off at that frequency in order to reduce the risk of instability which is applied in the frequency domain. This corresponds to the procedure reported by Møller et al. [1995].

3.8 Results

Figure 3.16 provides an example of HRTFs and HRIR at both ears for a sound source located at $\theta = 90°$, and $\varphi = 0°$ for subject 1.

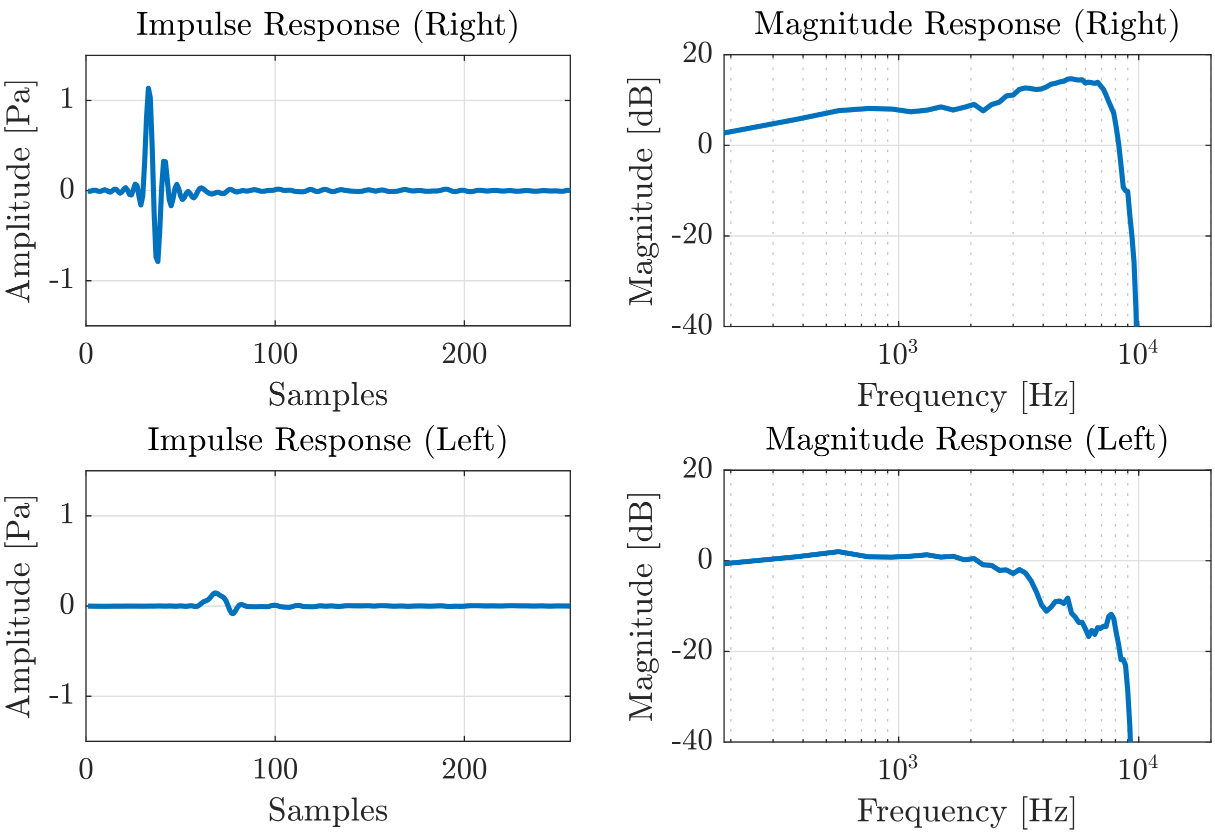

Figure 3.16: Example of HRIR and HRTFs on left and right ear for a sound source located to the right of the subject ($\theta = 90°$ and $\varphi = 0°$). The example was obtained on subject 1.

As expected, the signal at the ear closest to the source is stronger than that of the ear further away which demonstrates the ILD. The ITD can also be seen as the impulse response arriving ≈ 0.7 ms later than that of the right ear. In addition to that, the magnitude response of the left ear looks like a low-pass filter due to the shadowing effects of the head. The positive magnitude above 0 dB for the right hand side corresponds to pressure build-up and diffraction around torso, head and pinna [Blauert, 2005].

The HRTFs can be illustrated as a function of both frequency as well as azimuth which can be seen in figure 3.17. This example is generated from 57 azimuth locations for the middle speaker corresponding to $\varphi = 0°$.

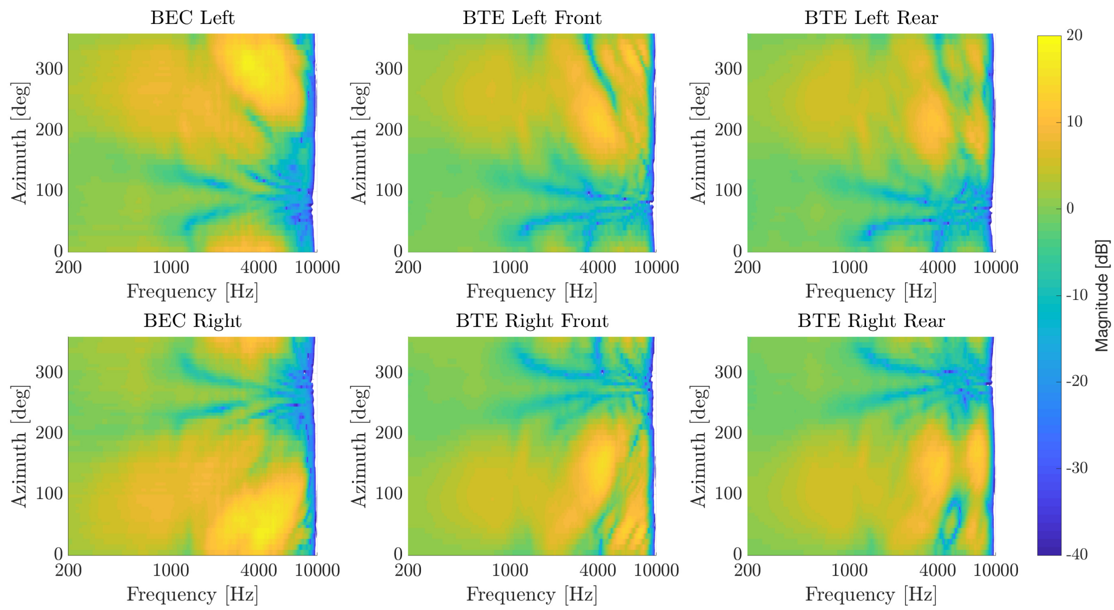

Figure 3.17: HRTF measurements as a function of frequency and azimuth for subject 1 for $\varphi = 0°$ for the blocked ear canal and at the behind the ear hearing aid for both ears.

The structures of the HRTF for the blocked ear canal corresponds well with similar representations reported by Minnaar et al. [2005]. On the contralateral side of each measurement position a funnel-like structure is seen and a directional gain pattern on the ipsilateral side. This is indicating that the HRTFs are measured according to the methods described by the literature hereby making the measurements of the current thesis comparable these. In addition to that, the HRTF measurements to the microphone positions of the hearing aids also show this funnel-line structure on the contralateral side but with a noticeable difference on the ipsilateral side. Based on the analysis of the 1999 dataset (figure 2.2 and figure 2.2) the difference between the blocked ear canal and the position of the BTE-HA is expected.

Similar plots as figure 3.17 for all 11 elevations for subject 1 can be found in Appendix A. In addition to that, plots for all 4 subjects for all 11 elevations can be found and studied in Appendix B.

4 | Directionality of Hearing Aids

Multiple microphones are usually a part of a modern day hearing aid that will allow for application of beamforming algorithms and thus present a directionally dependent signal. The application of the beamformer could be seen as an attempt to create an "artificial pinna" effect. Development and simulation of the directionality of a simple beamformer would offer an realistic reference to the constructed pinna reconstruction transfer functions.

This chapter is to describe the development and simulation of a simple first-order subtractive beamformer and the comparison of the directivity patterns to those of the blocked ear canal. In addition to that a comparison between the beamformer and pinna reconstruction filters will be made in the last section of the chapter.

4.1 Delay-and-Sum Beamforming

This section is to describe the derivation of a delay-and-sum beamformer, evaluate its performance before being compared to the directivity pattern of the blocked ear canal and to the pinna reconstruction filters which still is to be described.

Dillon [2012] describes the delay-and-sum beamformer as being the most commonly achieved method to create directivity of two omni-directional microphones by delaying and subtracting one output from of the other. More advanced methods of beamforming do exist but is beyond the scope of the thesis. The delay-ands-sum beamformer is deemed to offer a well established reference for applying directivity in hearing aids. The derivation for the beamforming equations are based on the assumption of the front and rear microphones are in a free field scenario with far field sources, hence we assume plane waves. This also means that it is assumed the shell of the hearing aid doesn't influence the measured acoustic signals and the microphones are identical.

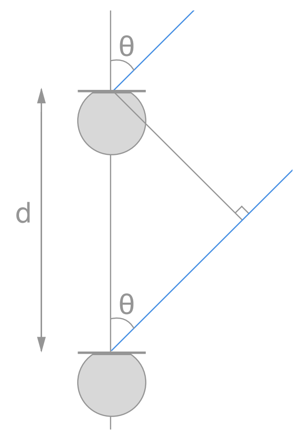

Figure 4.1: Sketch of microphone planement spaced with the distance d from a top-down view. Blue lines indicates the incoming plane wave from an angle θ.

For a plane wave with an angle of incedence of θ the time delay between the first microphone, m_1 and second microphone, m_2, is given by

$$\Delta\tau = \frac{d}{c} \cdot cos(\theta) \tag{4.1}$$

where: d : Distance between microphones

c : Speed of sound

The subtractive beamforming system is described by:

$$M_1 - D \cdot M_2 = Y \tag{4.2}$$

where: M_1, M_2 : Microphone signals in the frequency domain

D : Beamforming steering vector

Y : Beamforming output

The microphones M_1 and M_2 can be substituted but amplitude and phase:

$$A_1(f)e^{-i\varphi_1(f)} - D \cdot A_2(f)e^{-i\varphi_2(f)}e^{-i2\pi \cdot d/c \cdot cos(\theta)} = Y \tag{4.3}$$

where: A_1, A_2 : Frequency dependent amplitudes

φ_1, φ_2 : Phase shifts

θ : Angle of incidence of incoming wavefront

Following equation is true as one of the assumptions is there is no diffraction by the hearing aid shell and the response of the microphones are identical:

$$A_1(f)e^{-i\varphi_1(f)} = A_2(f)e^{-i\varphi_2(f)} \tag{4.4}$$

This reduces eq. 4.3 to:

$$1 - D \cdot e^{-i2\pi \cdot d/c \cdot cos(\theta)} = \frac{Y}{M_1} \tag{4.5}$$

Using eq. 4.5 an angle of no signal output of the beamformer can be defined by letting Y=0. The beamforming steering vector is therefore given by:

$$D = e^{i2\pi \cdot d/c \cdot cos(\theta_z)} \tag{4.6}$$

where: θ_z : Beamformer angle of maximum attenuation

The beamformer for $\theta_Z = \pi$ can be written as:

$$B(\theta) \cdot M_1 = Y \tag{4.7}$$

where

$$B(\theta) = (1 - e^{-i2\pi \cdot d/c} \cdot e^{-i2\pi \cdot d/c \cdot cos(\theta)}) \tag{4.8}$$

The final step of the beamforming design process is to ensure the correct gain is preserved for a given direction θ_p:

$$|\widehat{B}(\theta_p)| = |B(\theta_p) \cdot H| = 1 \tag{4.9}$$

where H is a correction to be designed for eq. 4.9 to be true:

$$|H| = \frac{1}{|B(\theta_p)|} \tag{4.10}$$

An filter design for H filter for $\theta_z = 180°$ and $\theta_p = 0°$ were created using MATLABs *fir2.m* and can be seen in figure 4.2.

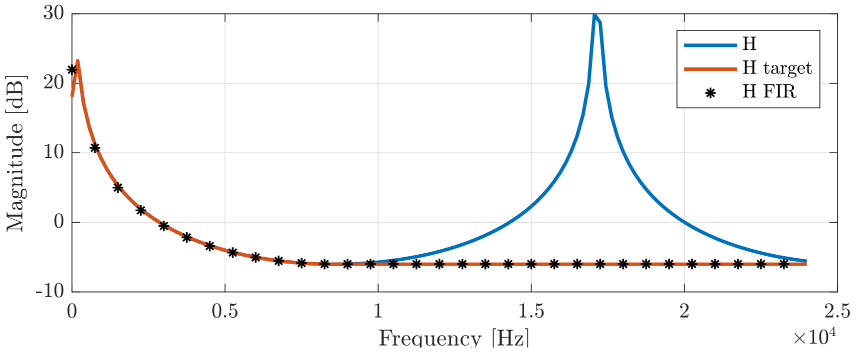

Figure 4.2: Gain preservation filter design using fir2 in MATLAB for a beamformer designed with the parameters $\theta_z = 180°$ and $\theta_p = 0°$.

It was chosen to manually flatten the filter response above 10 kHz to keep the filter order low while maintaining a good FIR approximation. An alternative to creating a linear phase filter could be to do a minimum phase representation of $B(\theta_p)$ as this would always have a stable inverse. Minimum phase reconstruction will be explained in more detail in section 5.4.

The resulting direcitivy patterns for the output is simulated for $\theta_z = 90°$, 135° and 180° for a microphone spacing of 1 cm and $\theta_p = 0°$. These patterns can be seen in figure 4.3.

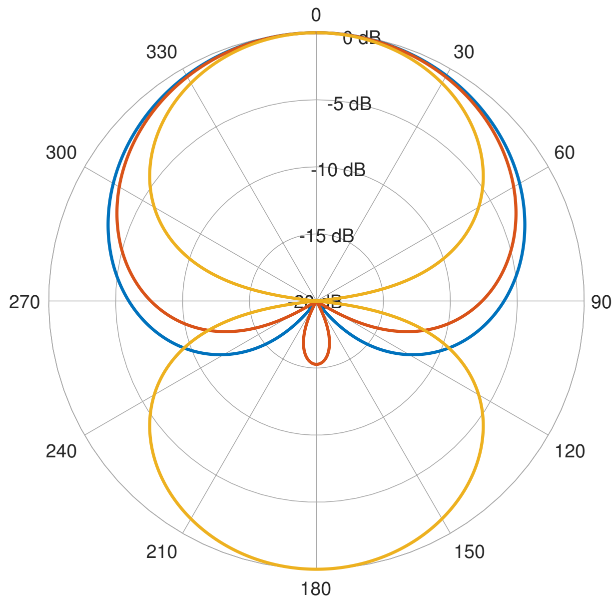

Figure 4.3: Resulting beamforming directivity plots for $\theta_z = 180°$ (blue) being a cardioid pattern, $\theta_z = 135°$ (red) being a hypercardioid pattern and $\theta_z = 90°$ (purple) being bi-directional (also called figure-eight pattern).

For $\theta_z = 180°$ a cardioid directivity pattern is obtained which will attenuate the most for sounds coming from the behind and some from the sides. It is also seen the gain is preserved for $\theta_p = 0°$. By choosing $\theta_z = 135°$ a hypercardioid directiviy pattern is created and for $\theta_z = 90°$ a figure-eight pattern is made, also called a bi-directional pattern as it focus in two directions being frontal and rear incidence.

Fractional Delay

To implement the subtracted beam forming design as described in section 4.1 one microphone signal is to be delayed and subtracted with the signal of the other. At a sampling frequency of 48 kHz a delay of 1 sample is 20.83 μs. For microphones spaced at 1 cm the traveling delay is 29.15 μs (for a speed of sound being 343 m/s) corresponding to $\approx$ 1.4 samples delay.

A fractional delay can be realized using the thiran aproximation as described by Laakso et al. [1996]. Figure 4.4 illustrates the group delay for the thiran approximation all-pass filter that results in 1.4 samples delay for order N=2 (blue) and N=6 (red).

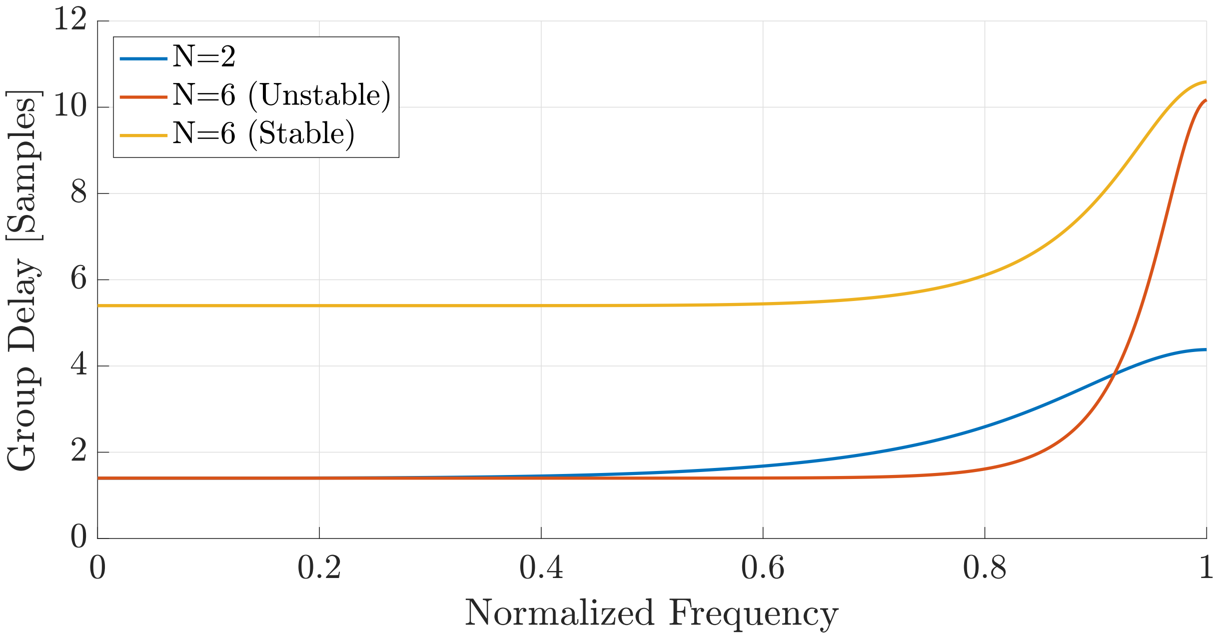

Figure 4.4: Group delay of the thiran approximation for N=2 (blue), N=6 but unstable (red) and stable version of N=6 (yellow) by increasing the group delay with 4 samples.

It can be seen that one can't expect 1.4 samples group delay for all frequency but the valid region expands as the order increases. If the order is increased to N=6 the filter becomes unstable. A solution could be to increase the group delay with 4 samples (yellow line) and delay the other microphone the same amount. The total group delay between the microphones will then be 1.4 samples but with a larger frequency span of use-ability. By doing this the overall group delay would be increased.

Validation of Beamformer Performance

This section is to evaulate the performance of the delay-and-sum beamformer and validate the gain correction filter that ensures 0 dB gain for θ_p.

A white noise source was simulated to be placed $\theta = 0°$, $90°$ and $180°$ relative to the beamformer. Uncorrelated white noise is applied to each microphone to simulate electrical noise.

The beamformer has its zero at 180° and the gain preservation filter is design using MATLABS *fir2.m* function in order to preserve the gain for sound sources placed at 0°. The power spectral density (PSD) of the output of the beamformer is illustrated in figure 4.5.

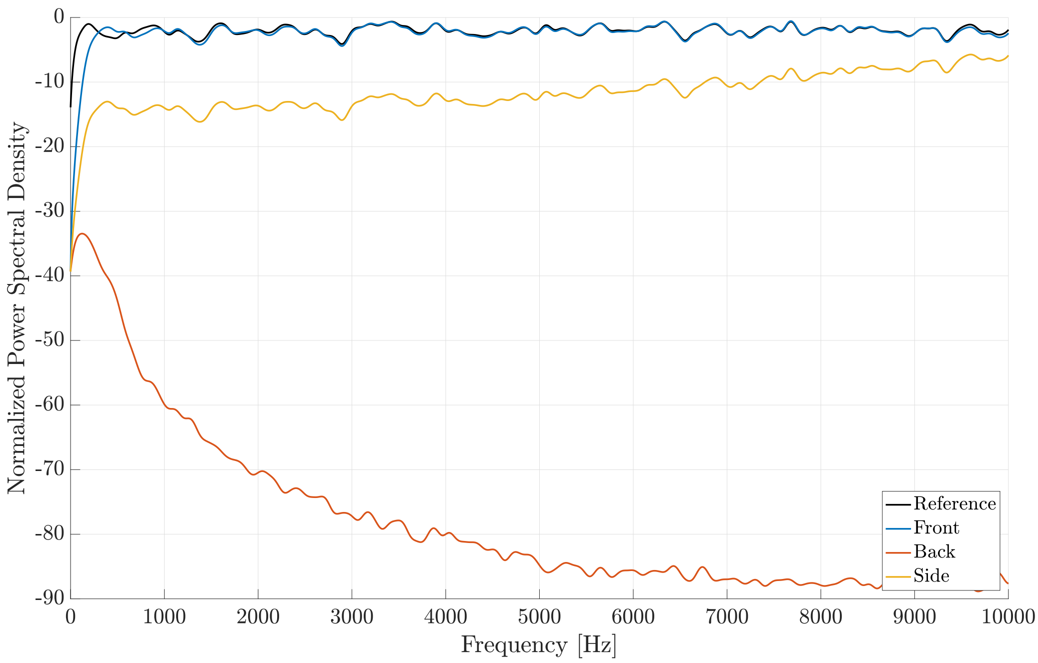

Figure 4.5: Power spectral density of the beamforming output for three chosen angles of incidence to the beamforming array which are compared to that of the reference signal. Indence from the side (yellow) is 90° and back is at 180°.

The black line represents the PSD of the reference noise signal and the blue being the output PSD of the beamformer for the noise source placed in front. Here it is seen that the gain is preserved f>1kHz and hereby validates the design of the gain preservation filter. The deviations between reference and ideal output f<1kHz is the contributions to the filter design of the gain preservation filter. In addition to that it can be seen that the sound source from 90° is attenuated $\approx$ 15 dB. For the sound source placed at the angle of the null a greater attenuation is observed and is increasing with frequency. For this example one of the downfalls of the design is seen which is the low frequency boost caused by the summation of the uncorrelated microphone noise. This is in agreement with the disadtantages stated by Dillon [2012] being an increased internal noise when used in quiet places. A method to avoid the low frequency noise boost could be to apply beamforming for frequencies greater than e.g. 1 kHz.

4.2 Pinna Reconstruction Transfer Function

This section is dedicated to define the pinna reconstruction transfer function which is based on the findings during the analysis of the 1999 database as described in section 2.3.

It was previously described that the difference between the BTE-HA microphone and the blocked ear canal was given by:

$$H(\theta, \varphi, k) = \frac{\mathrm{HRTF}_{BEC}(\theta, \varphi, k)}{\mathrm{HRTF}_{BTE}(\theta, \varphi, k)} \tag{4.11}$$

The pinna reconstruction transfer function (PRTF) will be describing the changes in magnitude and is therefore given by:

$$\mathrm{PRTF}(\theta, \varphi, k) = \left| \frac{\mathrm{HRTF}_{BEC}(\theta, \varphi, k)}{\mathrm{HRTF}_{BTE}(\theta, \varphi, k)} \right| \tag{4.12}$$

where: HRTF_{BEC} : The head-related transfer function at the blocked ear canal

HRTF_{BTE} : The head-related transfer function at the behind the ear hearing aid

An example of an PRTF using the BTE-HA front microphone as a function of frequency and azimuth can be found in figure 4.6 obtained at $\varphi = 0°$.

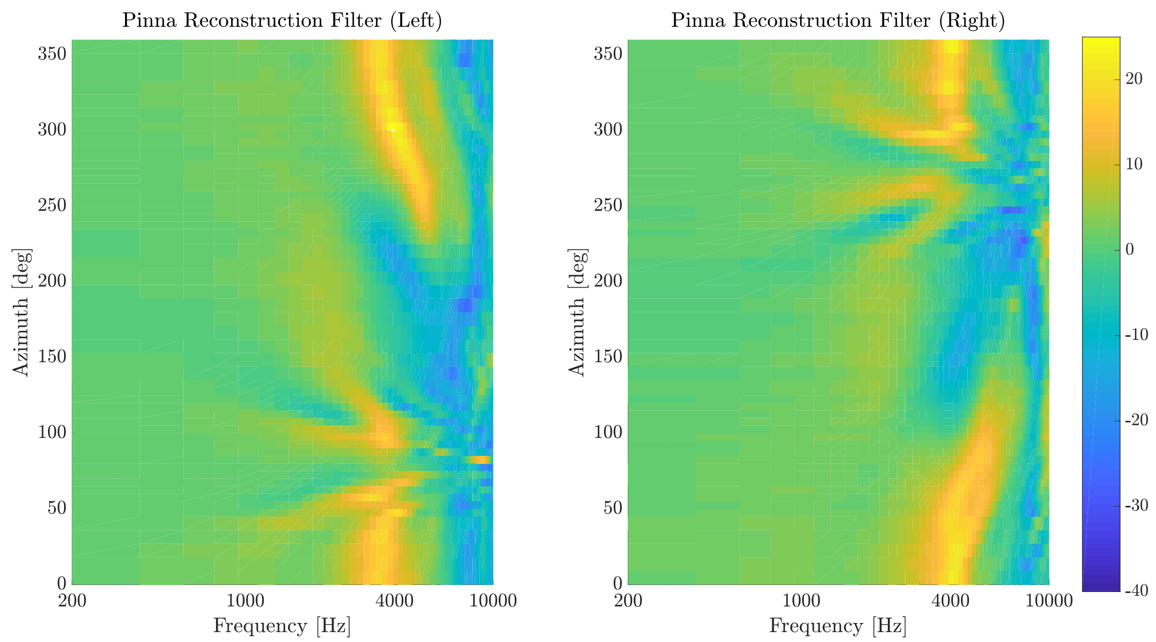

Figure 4.6: PRTF for both ears shown as a function of frequency and azimuth for subject 1. These are show for an elevation of $\varphi = 0°$.

In this figure the similar patterns to those observed in the analysis of the 1999 database and the validation experiment (see figure 3.7) can be seen for $\theta = 0°$ to $180°$.

In Appendix C the PRTFs for subject 1 can be found the all 11 measured elevations and a collection for all four subjects can be found in Appendix D.

The analysis of the pinna reconstruction transfer functions and their directivity patterns will be performed in the frequency domain in which they are defined. Explanation of transforming these into pinna reconstruction filters in the time domain is to be explained in section 5.4.

4.3 Beamformer and PRTF Directionality

This section is to investigate the effects of HRTFs on the ideal beamforming directivity patterns and compare these to the natural directivity of the HRTFs obtained at the blocked ear canal. In addition the directivity of the PRTFS will be compared to a beamforming equivalent. The HRTFs of the right ear will be used for the examples given in the remainder of the chapter.

Including HRTFs in Simulation of Beamformer Directivity

In the following subsections the directivity patterns of the ideal beamformer will be simulated with and without inclusion of the measured HRTFs at the front and rear microphones of the hearing aids.

The measured HRTFs will be included in the beamformer as:

$$B_{\mathrm{HRTF}}(\theta, \varphi, k) = \mathrm{HRTF}_{M_1}(\theta, \varphi, k) - \mathrm{HRTF}_{M_2}(\theta, \varphi, k) \cdot D(\theta_z) \cdot H(\theta_p) \tag{4.13}$$

where: HRTF_{M_1} : Response measured at the front microphone

HRTF_{M_2} : Response measured at the rear microphone

D : Beamforming steering vector

θ_z : Steering vector zero angle

H : Gain preservation filter

θ_p : Beamformer gain preservation angle

Directionally of HRTFs

The directivity of the HRTFs measured at the blocked ear canal will provide a natural reference to the spatial information available for normal-hearing listeners and are found in figure 4.7 for 4 selected frequencies for all 4 subjects measued.

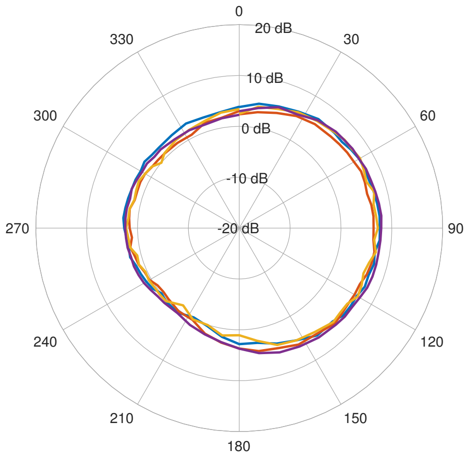

(a) f=500 Hz

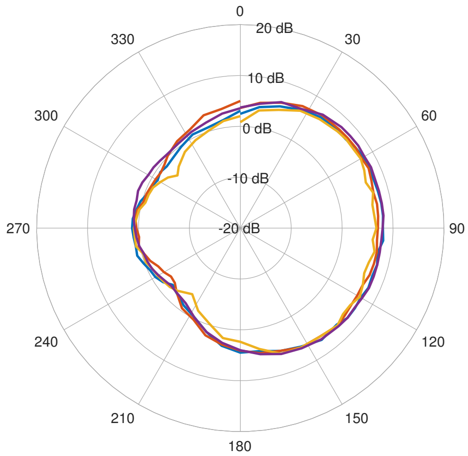

(b) f=1 kHz

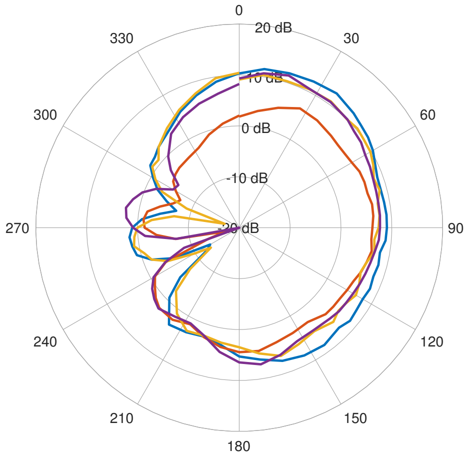

(c) f=2 kHz

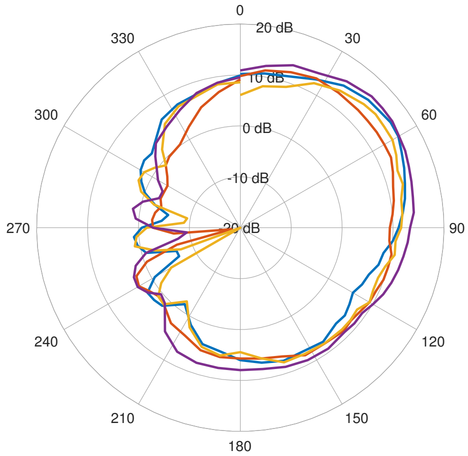

(d) f=3 kHz

Figure 4.7: Directivity plots for the blocked ear canal of all four subjects at selected frequencies of 500 Hz, 1 kHz, 2 kHz and 3 kHz obtained at an elevation of $\varphi = 0°$.

Slight discontinuities can be seen for $\theta = 0°$ which is due to the slight movements of the subjects. For the examples at 2 kHz and 3 kHz the effects of the head shadow is seen as an increased attenuated on the contralateral side of the head.

Directionally of Cardioid Beamformer

The ideal beamforming directivity with and without corrections by the measured HRTFs as described in eq. 4.13 with $\theta_z = 180°$ creating a cardioid pattern and $\theta_p = 0°$ which is shown in figure 4.8.

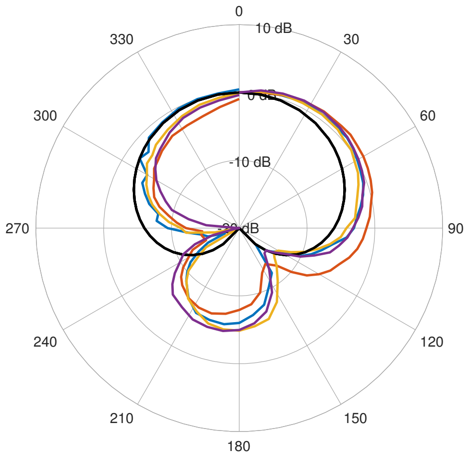

(a) f=500 Hz

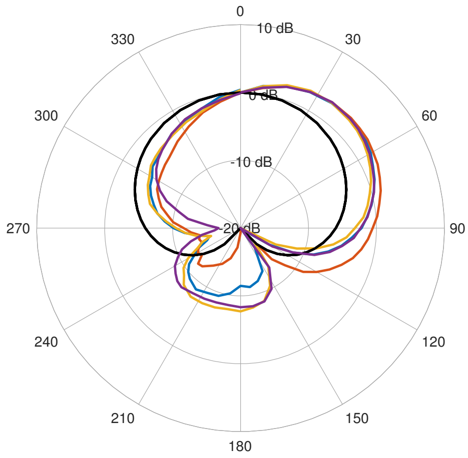

(b) f=1 kHz

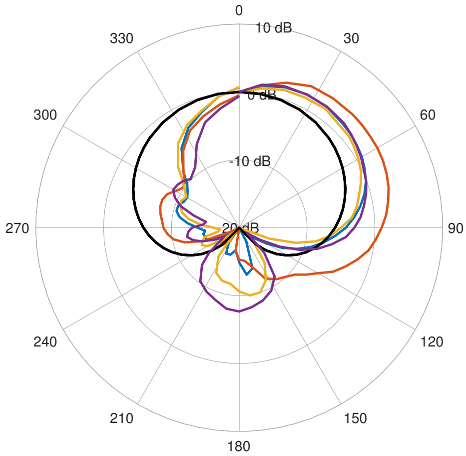

(c) f=2 kHz

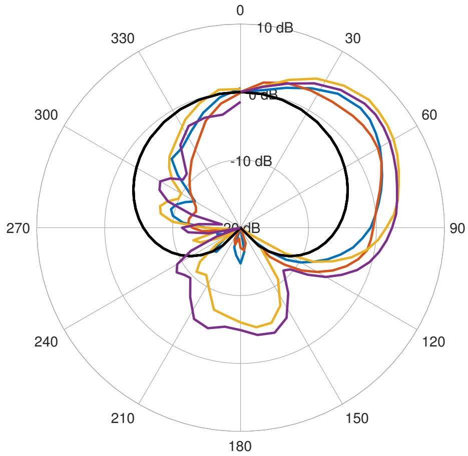

(d) f=3 kHz

Figure 4.8: Simulated beamforming patterns for $\theta_z = 180°$ (cardioid pattern) in the horizontal plane ($\varphi = 0°$) for the obtained HRTFs for the BTE-HA on the right side of the head of the 4 subjects who had HRTFs measured. Black line indicates the ideal beamformer and each color indicates the beamformer one of the four subjects.

On figure 4.8 the ideal beamforming pattern is simulated and compared to those where HRTFs are included. The result shows a steering towards to right and attenuation towards the left due to the head shadowing effects which increases with frequency. The resulting directivity would be categorized as being hypercardioid, indicating the simulated microphone distance of 1 cm might be slightly off the actual distance in the Widex Fusion hearing aids.

Directionally of Bi-Directional Beamformer

The ideal beamforming directivity with and without corrections by the measured HRTFs as described in eq. 4.13 with $\theta_z = 90°$ creating a bi-directional pattern and $\theta_p = 0°$ which is shown in figure 4.9.

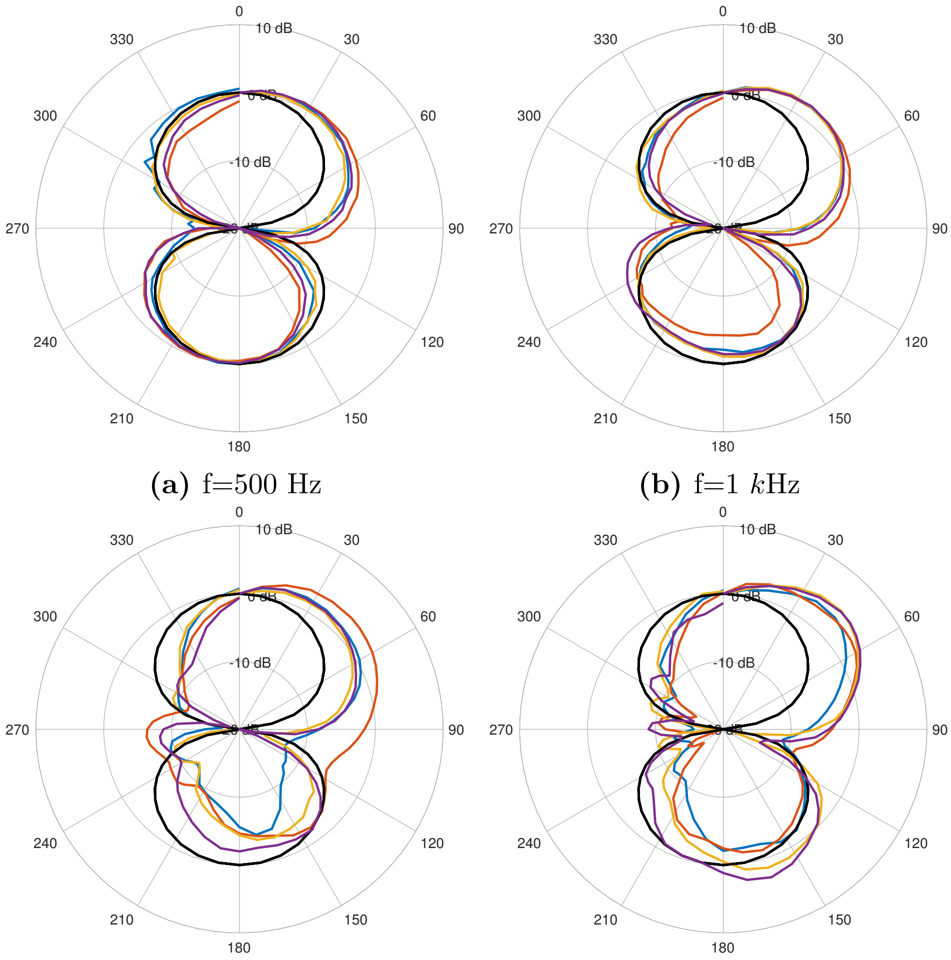

(a) f=500 Hz

(b) f=1 kHz

(c) f=2 kHz

(d) f=3 kHz

Figure 4.9: Simulated beamforming patterns for $\theta_z = 90°$ (bi-directional pattern) in the horizontal plane ($\varphi = 0°$) corrected by the obtained HRTFs for the BTE-HA on the right side of the head of the 4 subjects who had HRTFs measured. Black line indicates the ideal beamformer and each color indicates the beamformer one of the four subjects.

Similar effects as the cardioid simulation is seen for the bi-direcitonal case in figure 4.9.

Comparison of Beamformer and PRTFs

In this subsection a comparison will be made between the delay-and-sum beamformer and the proposed pinna reconstruction transfer functions. The beamformer to be compared with the PRTFs have been chosen to be a compromise between the cardiod and bi-directional patterns being a hypercardiod. This is accomplished by placing the zero and $\theta_z = 135°$.

The PRTF is to applied on one of the two microphones of the hearing aid, either M_1 (front) or M_2 (back). For this comparison the PRTF will be shown for

$$\text{PRTF}(\theta, \varphi, k) = \left| \frac{\text{HRTF}_{BEC}(\theta, \varphi, k)}{\text{HRTF}_{M_1}(\theta, \varphi, k)} \right| \tag{4.14}$$

These PRTFs will be compared to a "beamformer equivalent" given by:

$$B_{eq}(k, \theta, \varphi) = \frac{B_{\text{HRTF}}(k, \theta, \varphi)}{\text{HRTF}_{M_1}(k, \theta, \varphi)} \tag{4.15}$$

where B_{HRTF} is given by eq. 4.13.

The following two figures, figure 4.10 and figure 4.11 shows the directivity pattern from the beamformer and is compared to the directivity pattern of the pinna reconstruction transfer functions. The examples given at shown for f=1 kHz, 2 kHz, 4 kHz and 6 kHz and for three elevations at $\varphi = -40°$, $0°$ and $40°$.

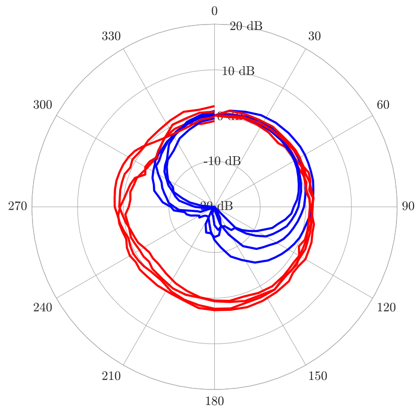

(a) f=1kHz, $\varphi = 40°$

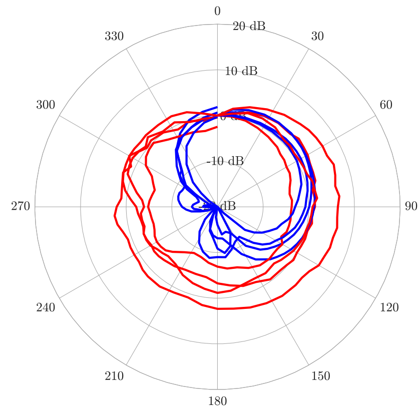

(b) f=2kHz, $\varphi = 40°$

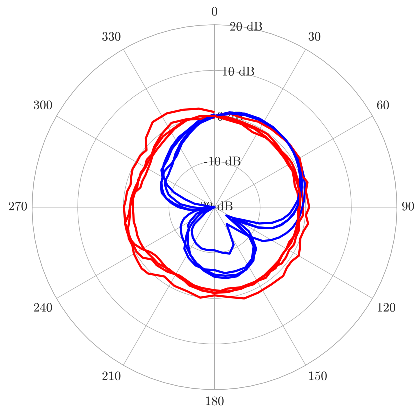

(c) f=1kHz, $\varphi = 0°$

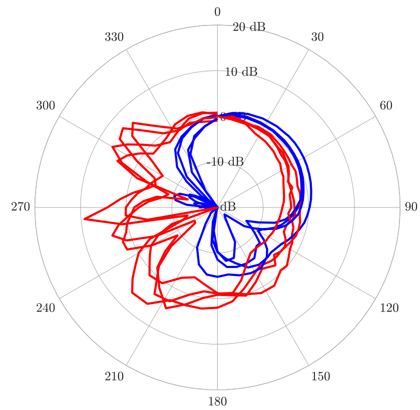

(d) f=2kHz, $\varphi = 0°$

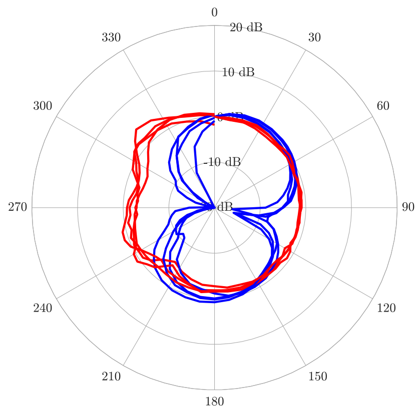

(e) f=1kHz, $\varphi = -40°$

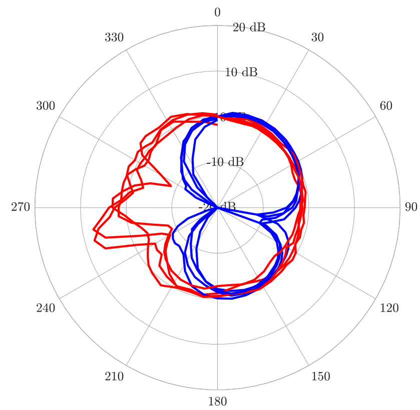

(f) f=2kHz, $\varphi = -40°$

Figure 4.10: Directivity plots for 2 kHz and 2 kHz for $\varphi = -40°$, $0°$ and $40°$. Blue lines are simulated beamforming patterns and red is the simulated PRTFs. Each line represents of one of four subjects measured.

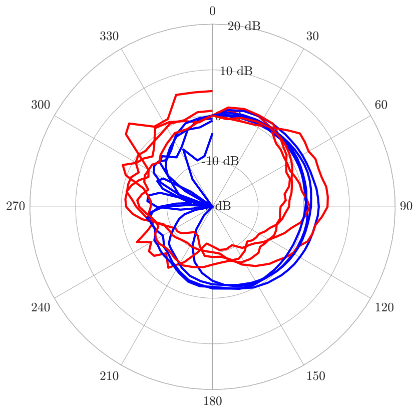

(a) f=4kHz, $\varphi = 40°$

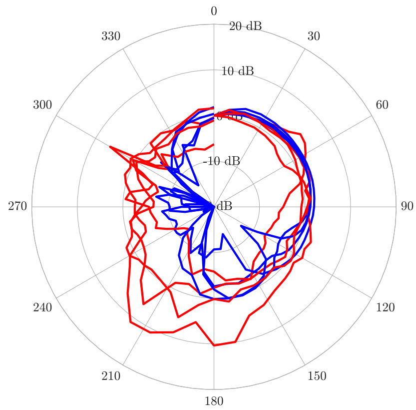

(b) f=6kHz, $\varphi = 40°$

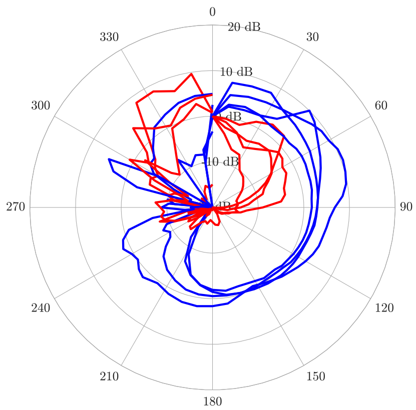

(c) f=4kHz, $\varphi = 0°$

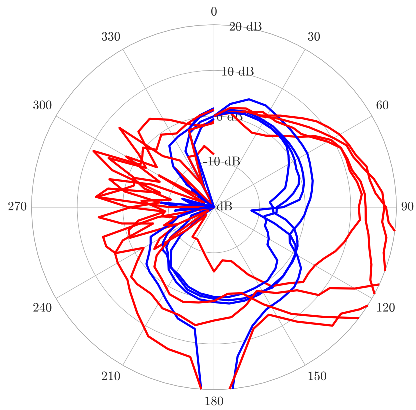

(d) f=6kHz, $\varphi = 0°$

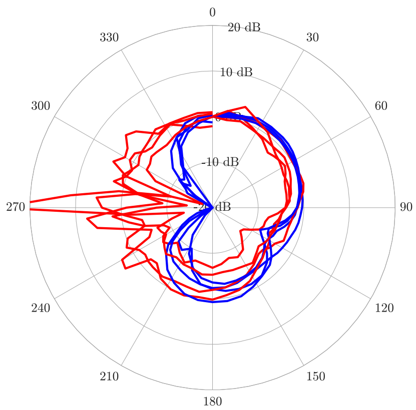

(e) f=4kHz, $\varphi = -40°$

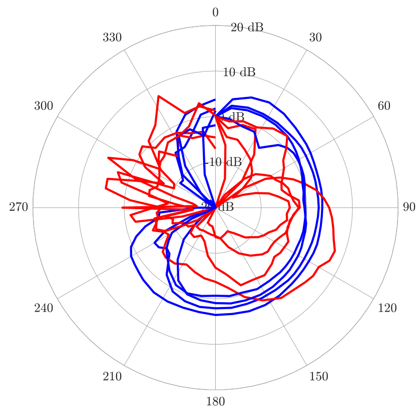

(f) f=6kHz, $\varphi = -40°$

Figure 4.11: Directivity plots for 4 kHz and 6 kHz for $\varphi = -40°$, 0° and 40°. Blue lines are simulated beamforming patterns and red is the simulated PRTFs. Each line represents of one of four subjects measured.

For the case at 1 kHz, seen in figure 4.10a, figure 4.10c and figure 4.10e, the directivity pattern of the beamformer does not change dramatically as a function of elevation as in the case of the PRTFs at 2 kHz seen in figure 4.10b, figure 4.10d and figure 4.10f. These difference between the delay-and-sum beamformer and the proposed PRTFs could indicate important elevation cues are lost for the beamformer.

Similar results are found at 4 kHz as seen in figure 4.11a, figure 4.11c and figure 4.11e. It is of interest how well the delay-and-sum beamformer approximates the PRTF for $\varphi = -40°$ found in figure 4.11e. It is also worth noting the change of directivity patterns of the PRTFs seems to be systematic for the four subjects. This is a general observation made for all three frequencies at which they are simulated.

At 6 kHz shown, seen in figure 4.11b, figure 4.11d and figure 4.11f, both the delay-and-sum and PRTF changes as a function of elevation. The PRTFs however seems to have a more unique and changing structure as a function of elevation and between subjects. This corresponds well with the fact that the variation seen in ordinary HRTFs increases with frequency where the wavelength no longer is no longer larger chance the dimensions of each unique pinna shape. It is could be indicated from these examples that the pinna reconstruction filters contains valuable and more complex localization cues for a change in elevation which corresponds well with the theory presented previously. Listening experiments should be carried out in order to validate wether or not the PRTFs could improve localization abilities for hearing aid users for changes in elevation.

5 | Real-Time Platform

In this chapter the design and development of the real-time platform, on which the PRFTs, or other types of hearing aid signal processing, can be implemented. The elements which has been included in the platform is shown in figure 5.1.

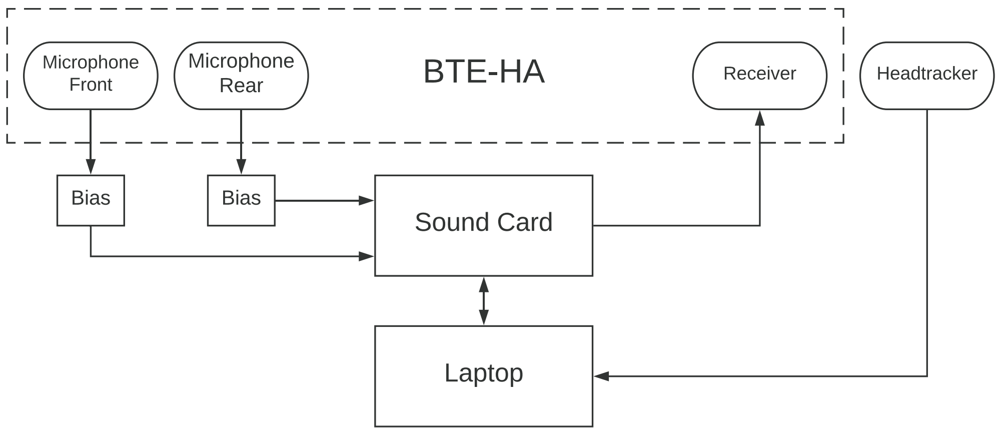

Figure 5.1: Real-time system concept.

The BTE-HA given contains front and rear microphones as well as one receiver as an output. The bias elements is the proprietary biasing circuitry as previously mentioned. The test platform is to sample the incoming sound from the microphones using a sound card connected to a laptop. The laptop is to process the signal digitally and play back the synthesized signal on the BTE-HA receiver using the sound card. The signal processing performed could be the implementation of the delay-and-sum beamformer, the PRFs etc. For the PRFs, the position of the sound source relative to the listener needs to be known. Head tracking therefore needs to be included to the system.

5.1 Software

MATLAB has been the programming and simulation tool of choice during the thesis and is therefore the first candidate of the software to be used for the real-time test platform. MATLAB will therefor allow for fast prototyping. The real-time element of the system requires low input/output latency as well as fast digital signal processing. Other software platforms such C or Python could be candidates on which to build the system but MATLAB is deemed adequate for the current phase of the project.

5.2 Head Tracking

As stated in section 2.5 one of the delimitations for the thesis work is that sound source positions is know for the processing of the sound so that the corresponding PRF can be applied. This requires head tracking hardware to provide the azimuth, elevation and roll of the head of the subject relative to the sound source.

The Polhemus FASTRAK magnetic tracking system was chosen to provide the head tracking angles. This system consists of a power supply, control box, an electromagnetic transmitter and a receiver. The receiver will be placed on top of the head of the subject. The transmitter transmits an oscillating magnetic field with a carrier frequency of 12 kHz [Polhemus, 2018]. The FASTRAK interfaces with the host computer via RS-232 to USB communication. A MATLAB "slave" script will be running continuously, reading the head tracking data from the USB serial port and via UDP send the head tracking data to the main MATLAB processing script. This was implemented in order to optimize head tracking data transfer so the main script is not halted due to head tracker update hereby creating audible artifacts.

5.3 System Latency

The processing system consists of a MacBook Pro (medio 2012 model) utilizing an RME UFX II sound card. The total I/O latency is desired to be as low as possible in order to maintain synchronization with head movement and visual stimuli.

The total latency for the real-time system is:

$$T_{total} = T_{system} + T_{process} \tag{5.1}$$

where: T_{system} : Latency through sound card, laptop (USB, drivers etc.)

$T_{process}$: Processing time (head tracking, interpolation, filtering etc.)

According to Groth and Søndergaard [2004] a 10 ms latency is rated as more annoying than e.g. 2- or 4 ms latency. A 10 ms is however still rated low on annoyance and is below what was to be rated as "disturbing". Furthermore, in real-life scenarios, reverberation would mask perceptual effects if the overall latency is below 10 ms. In a study performed by Sandvad [1996] a localization experiment were performed in virtual reality (VR) using binaural synthesis and a magnetic head tracker. Localization performance were evaluated for the system latency, the update rate of the head tracker and the spatial resolution of the obtained HRTFs. It was found that latencies exceeding 96 ms severely degrades the localization performance and at 29 ms the localization performance were close to real life localization. Furthermore, changing the head tracking update rate from 60 Hz (the fastest setting) to 20 Hz only had a small influence on performance. At 6 Hz localization changes in azimuth began to be affected. The author reported the switching between filters were audible for fast head movements for update rates at 20 Hz and lower.

For the present work it is desired to obtain a system latency less than 29 ms and a worst case head tracking update at 20 Hz. To explore in I/O latency of the system MATLABs *audioLatencyMeasurementExampleApp.m* was utilized. The system latency has been measured using various buffer sizes and sampling frequencies. The results of the measurements are found in figure 5.2.

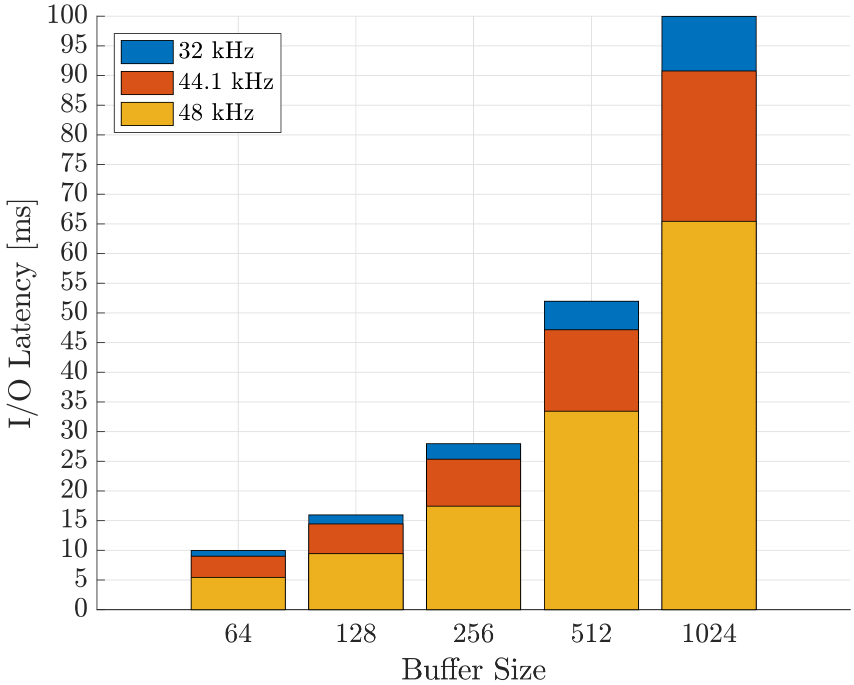

Figure 5.2: Measured T_{system} as a function of buffer sizes and sampling frequencies. Measured on a Macbook Pro medio 2012 running MATLAB 2017b interfacted to a FireFace UFX II sound card.

As expected, smaller buffer sizes as well as higher sampling frequencies results in lower system latency. A buffer size of 256 samples at 32 kHz sampling frequency or 64/128 samples at any of the test sampling frequencies is the upper limit to obtain a system latency less than 29 ms.

5.4 Design of Pinna Reconstruction Filters

The pinna reconstruction transfer functions will be transformed into time domain to actual pinna reconstruction filters (PRFs). These filters will be implemented as FIR filters and for the time being kept at a length of 256 corresponding to the length of the truncated measured impulse responses. When the PRFs are implemented on the BTE-HAs, the ITD will be included in the sampling of the microphones of the hearing aids. A minimum phase reconstruction will avoid simulating double ITDs. The use of the real cepstrum to obtained the minimum phase reconstruction is explained in the following section.

Minimum Phase Reconstruction

A non-minimum-phase and causal sequence can be presented as:

$$x[n] = x_{min}[n] * x_{ap}[n] \tag{5.2}$$

where: x_{min} : minimum-phase sequence

x_{ap} : Allpass sequence

It was showed by Plogsties et al. [2000] that the HRTF can be decomposed into:

$$H(z) = H(z)_{\text{minimum phase}} \cdot z^{-n} \tag{5.3}$$

where: $H(z)$: The HRTF in z-domain

$H(z)_{\text{minimum phase}}$: HRTF decomposed into its minimum phase representation

z^{-n} : n samples delay

Mehrgardt and Mellert [1977] showed similar results that the HRIR is approximately minimum-phase up to 10 kHz.

We see from eq. 5.3 that the amplitude of HRTF is that of the minimum phase component.

$$|H(z)| = |H_{min}(z)| \tag{5.4}$$

Due to the nature of minimum phase filters the filter is uniquely determent from either the phase or the amplitude. Using the real cepstrum the minimum phase filter can be reconstructed from its amplitude.

The real cepstrum is defined as:

$$c_x[n] = \mathcal{F}^{-1}\{log(|\mathcal{F}\{h[n]\}|\} \tag{5.5}$$

where: $\mathcal{F}\{\cdot\}$: Fourier transformation operation

h : Impulse response to be process

Oppenheim and Schafer [1975] showed that from the real cepstum the complex cepstrum corresponding to the minimum phase filter could be constructed by applying a window, l_{min}, to the real cepstrum.

$$\widehat{x}_{min}[n] = c_x[n] \cdot l_{min} \tag{5.6}$$

where

$$l_{min}(n) = \begin{cases} 1 & , \ n = 0, N/2 \\ 2 & , \ n = 1, 2, ..., (N/2) - 1 \\ 0 & , \ n = (N/2) + 1, ..., N - 1 \end{cases} \tag{5.7}$$

from the complex cepstrum the minimum phase filter can be calculated as:

$$x_{min}[n] = \mathcal{F}^{-1}\{exp(\mathcal{F}\{\widehat{x}_{min}[n]\}\} \tag{5.8}$$

This is implemented in the MATLAB function *rceps.m* and will be used to obtain the minimum phase reconstruction of measured HRIRs.

The minimum phase representation has, beside having a minimum phase characteristics, the exact same magnitude response as the obtained HRIR as shown in figure 5.3.

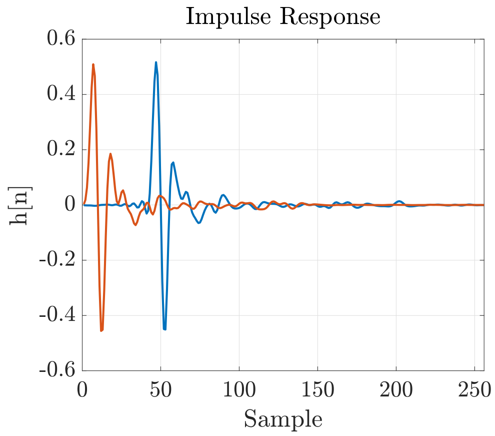

(a) Obtained HRIR (blue) and its minimum phase representation (red).

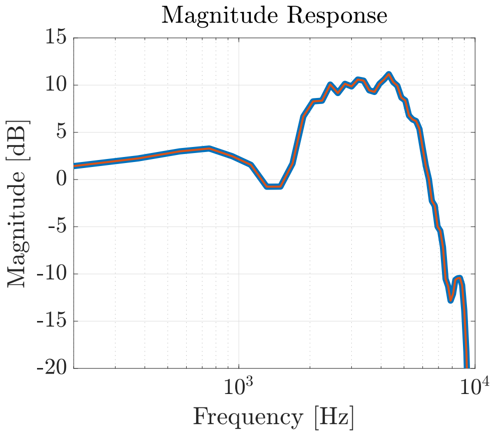

(b) Obtained HRTF (blue) and its minimum phase representation (red).

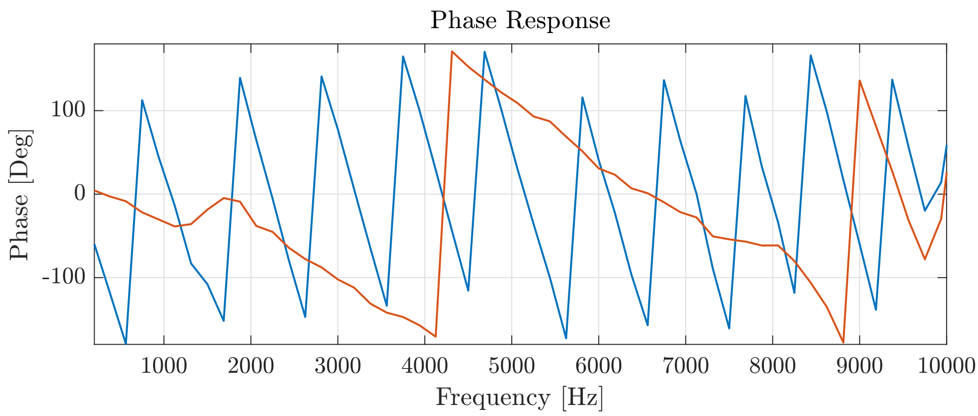

(c) Obtained phase (blue) and its minimum phase representation (red).

Figure 5.3: Obtained HRIR (blue) and its minimum phase reconstruction (red). As the minimum phase reconstructed HRIR has an equal magnitude response to that of the obtained HRIR one line is thicker than the other in the magnitude plot.

Inspection of the head-related impulse responses before and after the minimum phase reconstructions shows it almost corresponds to simply removing the initial delay of the impulse response.

5.5 Filter Implementation

MATLAB version 2017a and newer introduced *audioPlayerRecorder System object* which will be the recording and playback object used for implementation. An important feature of this object is the full control of choosing the buffer size. It was found in section 5.3 that a buffer size of 128 samples will result in $\approx$ 9.5 ms system latency at a sampling frequency of 48 kHz.

For an input sequence $x[n]$ with the length of N_x, the result of a convolution with the impulse response $h[n]$ of length N_h will result in an output sequence of $y[n]$ with length $N_y = N_x + N_h - 1$. Given $x[n]$ is 128 samples and the HRIR $h[n]$ 256 taps, the resulting convolution will be 383 samples. As the filter output is bigger than the output buffer size, the overlap-add method is utilized. Normally this method is used in order to convolve long input sequences but is useful in this thesis to implement buffer sizes smaller than the convolution length. The implemented overlap-add method is illustrated in figure 5.4.

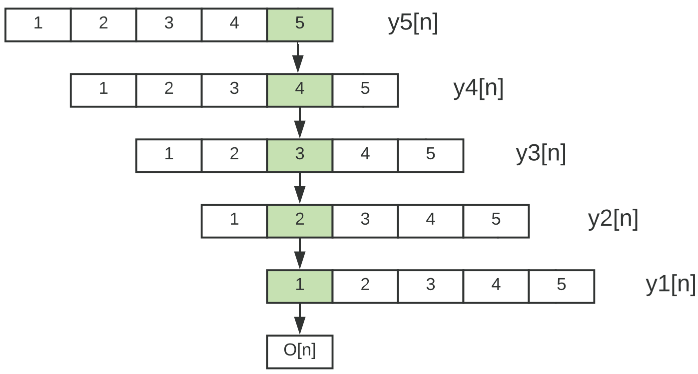

Figure 5.4: Illustration of the overlap-add method for a buffer size of 64. Convolution $y1[n]$ is the newest convolution and $y5[n]$ the oldest. The output sequence $O[n]$ is the sum of the frames colored in green.

For the illustrated example the buffer size, N_x, is 64 samples. This means the convolution output can be played over $N_B = 319/64 = 4.98$ buffers. This number of buffers is rounded up to the nearest interger.

The output sequence $O[n]$ is given by:

$$O[n] = \sum_{i=0}^{N_B - 1} y_{i+1}[iN_x + n], \quad n = 1, ..., N_x \tag{5.9}$$

where: N_x : length of input sequence (corresponding to buffer size)

N_B : Number of buffers required to output the convolved input sequence

$y_{i+1}[n]$: Convolution buffer

$i = 0$ corresponds to the newest convolution output. After convolution and computation of the overlap-add method given by eq. 5.9 the convolution buffer is shifted by 1 so that $y_2[n] = y_1[n]$, $y_3[n] = y_2[n]$ to $y_5[n] = y_4[n]$. For slow changes in the target position of the sound source the described method works well but whenever a large change in HRIR is made in a short amount of time, audible clicks can be detected. To minimize these artifacts, a moving average (MA) smoothing is applied to the HRIR.

5.6 Results

The results of development and implementation of this real-time platform has lead to a stable system on which real-time and dynamic binaural synthesis can be performed. The results of the real-time system therefore consists of block diagram of the implemented code blocks as well as the result of an informal listening test that evaluates the quality of the binaural synthesis platform.

MATLAB Implementation Flowchart

Figure 5.5 shows the block digram of the elements and processes included in the real-time simulation platform. Rounded boxes indicates information flowing from hardware into MATLAB. Hard-edge boxes indicates a digital signal processing blocked. Multiple-page box indicates the PRF database which is processed offline and prior to the test.

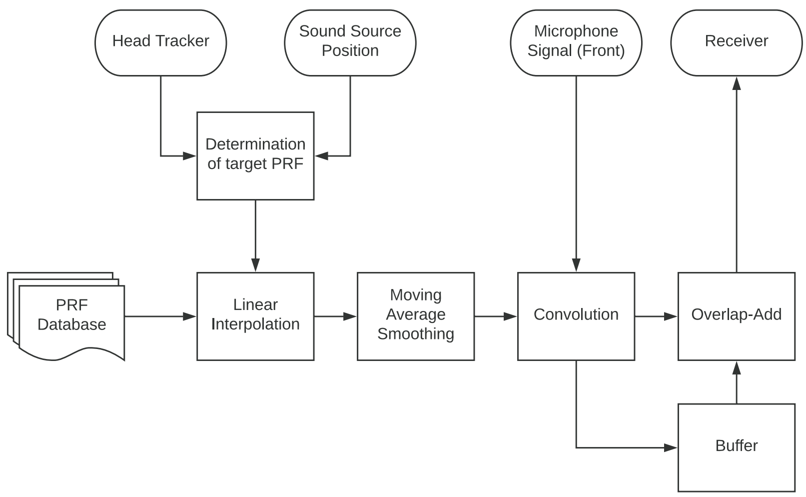

Figure 5.5: Block diagram of the elements that describes the major code blocks of the real-time implementation on which the localization performance of the PRTFs can be evaluated.

In the implemented system, the fetching of head tracking data is run by a separate MATLAB program and is parsed to the main processing script via UDP.

The block diagram shows the flow of the software which should be used when the localization performance of the PRTFs are to be evaluated. A similar framework can be used to create a platform on which beamforming algorithms or other hearing aid signal processing can be evaluated in real-time at a low latency.

Platform for Binaural Synthesis

During the work of the thesis the PRFs were synthesized but never deployed on the real-time platform using the hearing aids. Implementation of HRTFs for the blocked ear canal was was carried out in order to evaluate the performance of the real-time platform. For this purpose the stimuli was either white noise or music delivered to the subject via headphones.

Informal listning test was carried out by using the platform for real-time and dynamic binaural synthesis to validate the platform in fact could run as proposed in figure 5.5. During these tests it was found that the 256 tap filters could be implemented at a buffer size of 128 samples as utilizing the method as described in section 5.5. It was also found the implemented method allowed for smooth transition between filters whenever the head tracker provided a new angle.

One subject, being one of the four who had their HRTFs measured, provided a qualitative evaluation of the binaural synthesis platform. Whenever the sound source was moved in the horizontal plane at $\theta = 0°$, $90°$, $180°$ and $270°$ the subjected used the freedom of head movements to rapidly determine where the sound source were placed. The subject had however difficulty in localizing in the median plane which could be caused by the lack of headphone equalization.

The results of the informal listening test validates that the methods implemented to create the real-time platform works as intended and have given data and inspiration of improvements to the system which can be implemented in the future.

6 | Discussion

During the work of the thesis HRTFs to the blocked ear canal and the two microphones of a set of behind-the-ear hearing aids has been successfully obtained for 611 unique sound source positions around 4 human subject. From these HRTF measurements the pinna-reconstruction transfer functions directivity patterns have been obtained and compared to those of a delay-and-sum beamformer. Lastly an real-time simulation platform were developed and implemented on which localization performance can be evaluated for various types of signal processing methods. Due to the time constrains of the thesis the real-time platform were evaluated by using it as a means of performing dynamic binaural reproduction of prerecorded signals.

This chapter will contain descriptions and comments of the work carried out during the thesis period and give inspiration to what could be the next step of research within this theme.

6.1 Head-Related Transfer Functions

The work of the thesis is centered around measuring head-related transfer functions to the blocked ear canal as well as the two microphones of the widex fusion hearing aids. During development of the setup and during measurements of human subjects a number of observations which could be included if similar measurements are to be made in the future.

During synthesis of the head-related transfer functions it was found the plastic shielding of the hearing aids were to be removed from the housing in order to obtain reasonable reference measurements. After a discussing the finding with Flemming Christensen it was proposed that one removes the microphones completely from the hearing aid housing during the reference measurements. By doing this only the response of microphone is deconvolved hereby letting the resulting HRTF describe the hearing aid and its fitting on the subject fully. Removing of the hearing aid microphones were however not possible during the thesis work.

The hearing aids hangers provided by widex were delivered with high quality wires providing connections to both microphones and the receiver. When hearing aids are worn with the correct length of receiver and size of silicon molds no problems where found by having the external wires attached. During measurement of the HRTFs no receiver provided support of the hearing aid and were therefore placed behind the ear of the subject by the means of medical tape. Due to the heavy and stiff external wiring of the hearing aids they tended to move outwards and away from the skull. It is recommended to find a solution that allows for correct fitting of the hearing aids while maintaining the external wiring of the hearing aid hangers. The creation of the measurement harness did however reduce the strain of the wires and stability of the hearing aid placement during the 30 minute measurement period.

The code developed in MATLAB that controls the measurement flow and the MLS measurements themselves were created for this specific purpose. It was found that the measurement time to obtain the HRTFs for the 611 sound source locations could be reduced from 30 minutes to approximately 8 minutes. An issue in the sampling of data via the sound card where buffers could be skipped were experienced when trying to reduce measurement time. The 30 minute measuring time were accepted as it ensured no buffers were skipped and therefore properly time aligned. An optimization of the measurement software could either lead to fast measurement procedure of the 611 chosen sound sources or allow for even fine angular resolution in azimuth in the same 30 minute timeframe.

For the HRTF measurements during the thesis 11 speakers were spaced vertically from -40° to 40° elevation in 8° increments. The size of the speaker setup and their mounting in the anechoic room did lead to reflections noticeable in the impulse responses measured. These were however easily removed by time windowing the impulse responses. It has been throughout the thesis been seen that the HRTFs and PRTFs do change as a function of elevation which could lead to the idea of obtaining the HRTFs in an even finer angular resolution. For future measurements a new physical frame on which a single speaker is moved in very small steps could be implemented. This could result in a measurement setup in which HRTFs can be obtained at a very high angular resolution in both azimuth and elevation directions.

It was found during HRTF measurements that subjects had difficulties standing completely still throughout the 30 minute measurement session despite the fact small breaks were included. The proposed idea of using a laser and target disc to ensure correct position were never used as measurement time would increase manyfold. It is proposed that either stability of the subject is increased or an intelligent system is implemented to track the subject during measurements and redo these if out of position.

The pinna-reconstruction transfer functions were in the thesis created by HRTF measurements which is impractical in the case of real life implementation and use. An alternative to this could be to isolate the pinna by placing this in a baffle which is surrounded by multiple speakers. This idea and setup is described by Christensen et al. [2013]. The pros of such a setup is the complete isolation of the pinna from the rest of the body and its more practical physical setup. A major downside of the method is however the lack of response on the contralateral side as speakers are only mounted on the ipsilateral side of the baffle. One could explore how the contralateral responses could be estimated from the ipsilateral measurements. This method would also lead to less positioning problems as mentioned being a problem doing standing HRTF measurements.

6.2 Pinna Reconstruction Transfer Functions

Measurements performed by Christensen [1999] showed gain differences to be up to 30 dB between the microphones located behind the ear to the blocked ear canal. The findings lead to the idea of pinna reconstruction transfer functions and the thesis work of this thesis.

The HRTF measurements which were performed on four subjects made it possible to further investigate these pinna reconstruction transfer functions which describes the directional dependent differences between the hearing aid and the blocked ear canal in greater detail which was one of the motivations of the thesis.

The PRTFs created and explored during the thesis work corresponds well with those found in the analysis of the 1999 dataset and the grand goal of the thesis would have been to explore if the localization performance would be increased compared to e.g. a delay-and-sum beamformer. It did however prove to be an optimistic goal which is why the aim on the thesis was to explore the pinna reconstruction transfer function, compare these to known beamforming methods and to create a real-time platform on which they can be tested.

The evaluation of the obtained PRTFs were based on an analysis of the directivity patterns for a selected number of frequencies and angles of elevation. Here it was shown that the PRTF might contain more complex patterns when compared to a delay-and-sum beamformer. In order to explore the perceptual impact of the PRTFs a psychoacoustic localization experiment should be carried out using the developed real-time simulation platform.

6.3 Real-Time Simulation Platform

It was proposed by Mueller et al. [2012] that a virtual sound environment could be used in evaluating hearing aid algorithms as binaural synthesis can create a convincing sound environment in which localization abilities are preserved compared to real life. The concept was adapted by the current thesis and the recommendation of implementation of a motion tracker to allow for head movements were included in the development and implementation.

Being able to simulate hearing aid algorithms in a well-known simulation tool, such as MATLAB, in real-time at low latency including head movement information could be of great value to those designing af testing new hearing aid algorithms.

The real-time simulation platform created during the thesis were implemented in MATLAB based on being the mathematical tool of choice during the masters programme. Despite the fact that MATLAB is a mathematical analysis tool and by no means meant as being the engine to perform real-time audio processing at a low latency it was proved that dynamic binaural synthesis were possible using MATLAB 2017b on a 2012 MacBook Pro.

Future work on the real-time platform on which hearing aid algorithms can be tested in real-time could include either optimization of the current MATLAB framework or use the ideas and concepts in another programming language such as python which allows for multi-processing structures unlike MATLAB. Further optimization of the real-time platform could be reducing the system in/out latency and/or improvement of used magnetic motion tracking system used or even implement another motion tracking system. All these elements could improve the quality of the platform. The MATLAB implementation created during this thesis does however offer a working dynamic binaural synthesis platform on which future work can be based.

6.4 Perception of PRTFs

The localization performance of the pinna reconstruction filters were evaluated from simulations. A natural next step in evaluate these would be in psychoacoustic listening test utilizing the real-time simulation platform.

The PRFs can be evaluated in a number of ways. The aim of the thesis was to increase localization performance for users of behind the ear hearing aids. The first step in evaluating the PRFs could therefore be a localization experiment in order to evaluate horizontal localization, vertical localization and median plane errors. These results could be compared to unaided hearing listening and aided listening with and without beamforming algorithms applied.

In addition to that a more qualitative evaluation could be made where subjects were to rate e.g. naturalness, feeling of externalization etc. This could again be compared to the unaided hearing listening and aided listening with and without beamforming algorithms applied.

Bibliography

Outline ET 250-3D. ET 250-3D, 2018. URL http://outline.it/outline-products/measurement-systems/et-250-3d/.

anechoic room. Aalborg University, Department of Electronic Systems, 2018. URL http://doc.es.aau.dk/labs/acoustics/facilities/anechoic_room_large/.

D.W. Batteau. The role of the pinna in human localization. 168:158–80, 09 1967.

J. Blauert. *Communication Acoustics*. Springer, 1 edition, 2005.

W. Owen Brimijoin, Alan W. Boyd, and Michael A. Akeroyd. The contribution of head movement to the externalization and internalization of sounds. 8:e83068, 2013. ISSN 1932-6203. doi: 10.1371/journal.pone.0083068.

Flemming Christensen. Hrtf database from previously, non-published results. *Aalborg University*, 1999.

Flemming Christensen and Henrik Møller. The design of valdemar: an artificial head for binaural recording purposes. *Proceedings of the 109th Audio Engineering Society Convention, September 22-25, 2000, Los Angeles, California, USA Proceedings of the 109th Audio Engineering Society Convention, September 22-25, 2000, Los Angeles, California, USA*, 2000.

Flemming Christensen, Clemen Boje Larsen, and Henrik Møller. Measuring components of hrtfs. 1999.

Flemming Christensen, Pablo F. Hoffmann, and Dorte HammershÃži. Measuring directional characteristics of in-ear recording devices. In *Audio Engineering Society Convention 134*, May 2013. URL http://www.aes.org/e-lib/browse.cfm?elib=16784.

AAU Department of Electronic Systems. Acoustics Ballspeaker (small), 2018. URL http://doc.es.aau.dk/labs/acoustics/equipment/vifa_ball/.

H. Dillon. *Hearing Aids*. Thieme, 2 edition, 2012.

Mark B. Gardner and Robert S. Gardner. Problem of localization in the median plane: effect of pinnae cavity occlusion. *The Journal of the Acoustical Society of America*, 53(2):400–408, 1973. doi: 10.1121/1.1913336. URL https://doi.org/10.1121/1.1913336.

Jennifer Groth and Morten Birkmose Søndergaard. Disturbance caused by varying propagation delay in non-occluding hearing aid fittings. 43:594–599, 2004. ISSN 1499-2027. doi: 10.1080/14992020400050076.

H. L. Han. Measuring a dummy head in search of pinna cues. *J. Audio Eng. Soc*, 42(1/2):15–37, 1994. URL http://www.aes.org/e-lib/browse.cfm?elib=6964.

Ira J. Hirsh. Masking of speech and auditory localization. *Audiology*, 10(2):110–114, 1971. doi: 10.3109/00206097109072548. URL http://www.tandfonline.com/doi/abs/10.3109/00206097109072548.

Timo I. Laakso, Vesa Välimäki, Matti Karjalainen, and Unto K. Laine. Splitting the unit delay [fir/all pass filters design]. 13, 1996. ISSN 1053-5888. doi: 10.1109/79.482137.

S. Mehrgardt and V. Mellert. Transformation characteristics of the external human ear. 61: 1567–1576, 1977. ISSN 0001-4966. doi: 10.1121/1.381470.

P Minnaar, J.A.N. Plogsties, and Flemming Christensen. Directional resolution of head-related transfer functions required in binaural synthesis. 53:919–929, 10 2005.

Brian C J Moore. *An introduction to the Psychology of Hearing*, volume 0 of *10*. Brill, 6 edition, 0 2013.

Martin F. Mueller, Andrea Kegel, Steven M. Schimmel, Norbert Dillier, and Markus Hofbauer. Localization of virtual sound sources with bilateral hearing aids in realistic acoustical scenes. 131:4732–42, 2012. ISSN 1520-8524. doi: 10.1121/1.4705292.

Henrik Møller. Fundamentals of binaural technology. *Applied Acoustics*, 36(3/4):171–218, 1992. ISSN 0003-682X.

Henrik Møller, Michael Friis Sørensen, Dorte Hammershøi, and Clemen Boje Jensen. Head-related transfer functions of human subjects. *J. Audio Eng. Soc*, 43(5):300–321, 1995. URL http://www.aes.org/e-lib/browse.cfm?elib=7949.

Henrik Møller, Michael Friis Sørensen, Clemen Boje Jensen, and Dorte Hammershøi. Binaural technique: Do we need individual recordings? *J. Audio Eng. Soc*, 44(6):451–469, 1996. URL http://www.aes.org/e-lib/browse.cfm?elib=7897.

Alan V. Oppenheim and Ronald W. Schafer. *Discrete-Time Signal Processing*. 1975.

Jan Plogsties, Pauli Minnaar, S. Krarup Olesen, Flemming Christensen, and Henrik Møller. Audibility of all-pass components in head-related transfer functions. In *Audio Engineering Society Convention 108*, Feb 2000. URL http://www.aes.org/e-lib/browse.cfm?elib=9206.

Polhemus. 3SPACE FASTRAK USER MANUAL, 2018. URL https://polhemus.com/_assets/img/FASTRAK_User_Manual_OPM00PI002-G.pdf.

J. Sandvad. Dynamic aspects of auditory virtual environments. In *Audio Engineering Society Convention 100*, May 1996. URL http://www.aes.org/e-lib/browse.cfm?elib=7547.

Sonion. Sonion 8002, 2018. URL http://www.sonion.com/wp/wp-content/uploads/8002-2003357.pdf.

Jesper Udesen, Tobias Piechowiak, Fredrik Gran, and Andrew Dittberner. Degradation of spatial sound by the hearing aid. *Proceedings of the International Symposium on Auditory and Audiological Research*, 4:271–278, 2013. ISSN 2596-5522. URL https://proceedings.isaar.eu/index.php/isaarproc/article/view/2013-29.

Tim Van den Bogaert, Thomas J Klasen, Marc Moonen, Lieselot Van Deun, and Jan Wouters. Horizontal localization with bilateral hearing aids: Without is better than with. 119:515–26, 02 2006.

virmary. WhyNotShowOff, 2018. URL https://www.thingiverse.com/thing:1498115.

Widex. UNIQUE FUSION RIC/RITE, 2018. URL https://www.widex.dk/hearing-aids/unique-hearing-aids/productdisplay-unique#filterCategory=0&filterType=0&currentSlide=NaN&filterModel=4&colorPicker=0&colorGridPicker=-1.

Appendix

A | HRTF Measurement Results

This appendix contains all HRTF plots for subject 1 for all 11 elevations measured. HRTF plots for all 4 subjects can be found digitally in Appendix B.

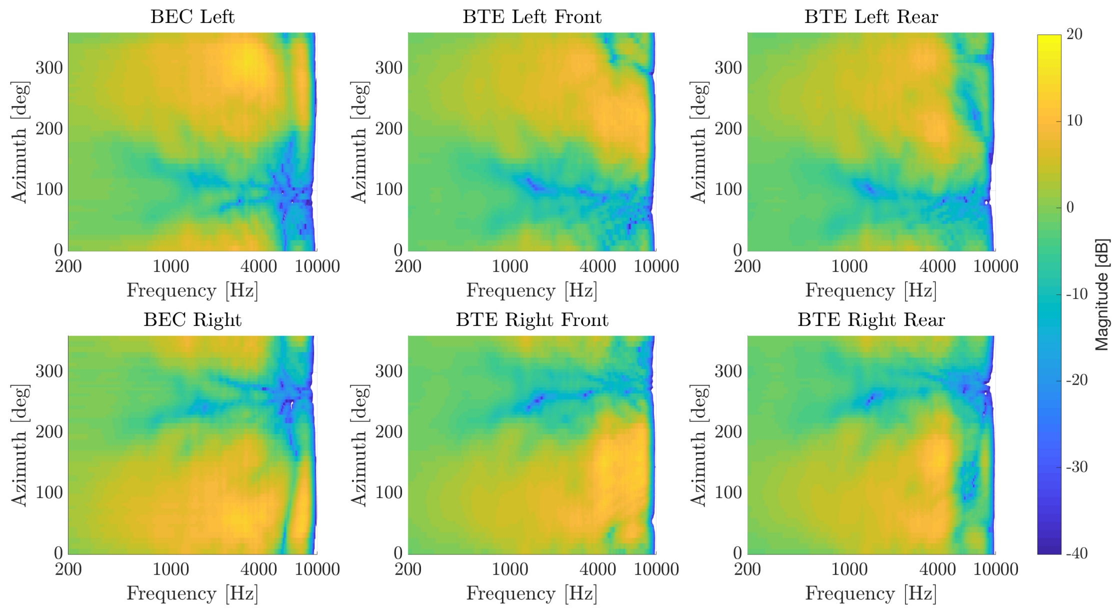

Figure A.1: Subject 1, $\varphi = -40°$

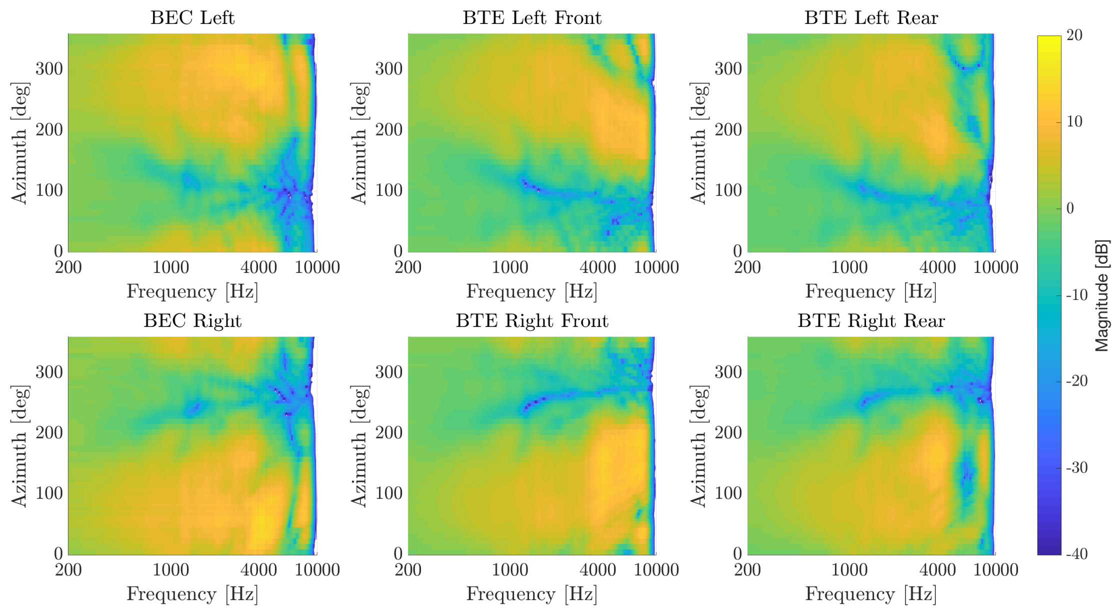

Figure A.2: Subject 1, $\varphi = -32°$

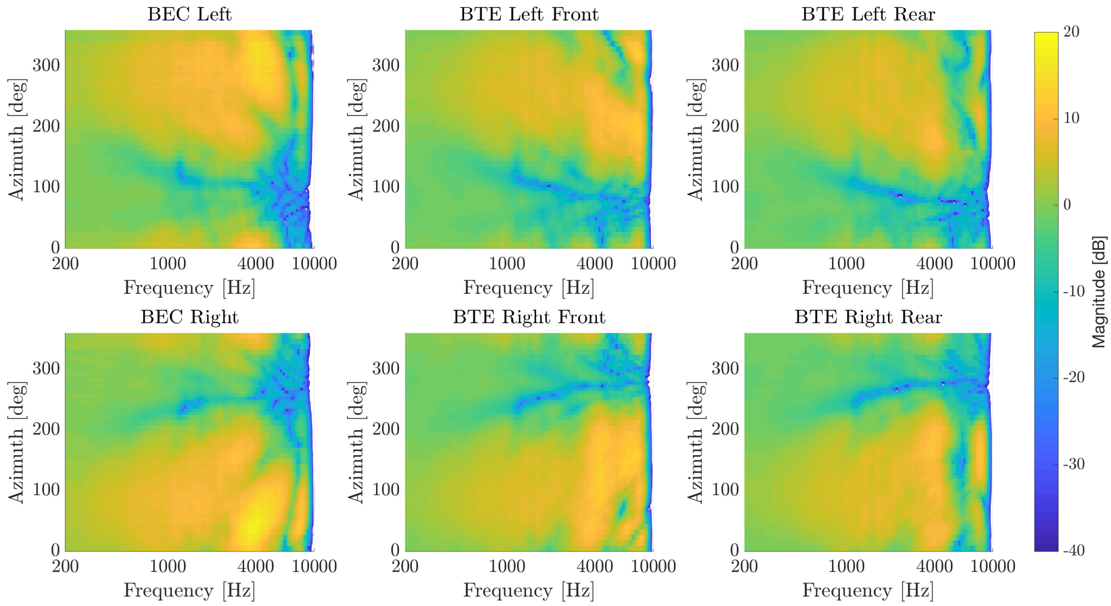

Figure A.3: Subject 1, $\varphi = -24°$

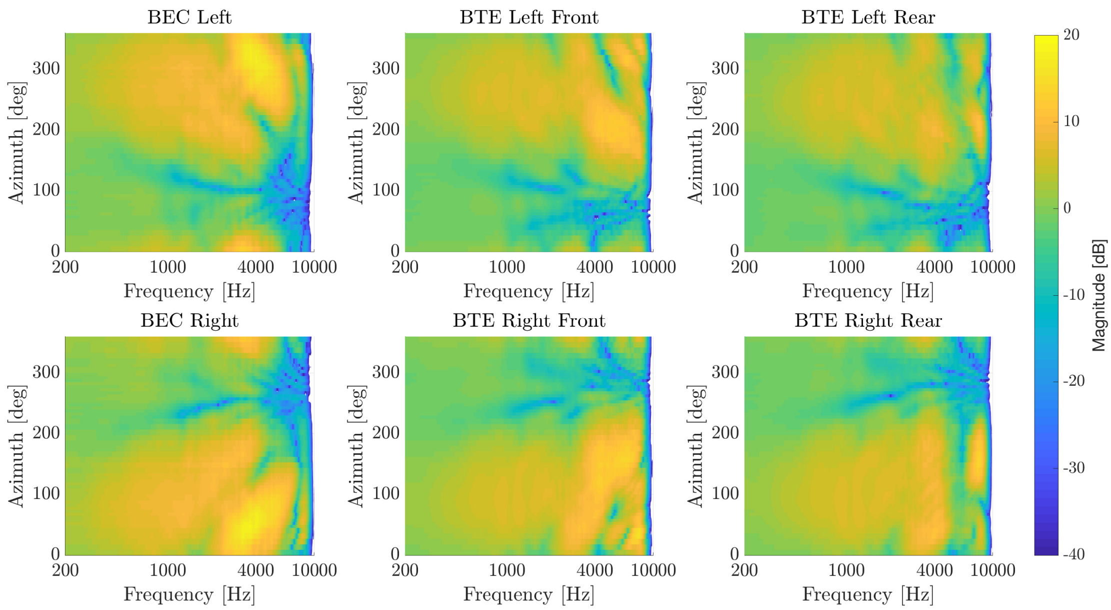

Figure A.4: Subject 1, $\varphi = -16°$

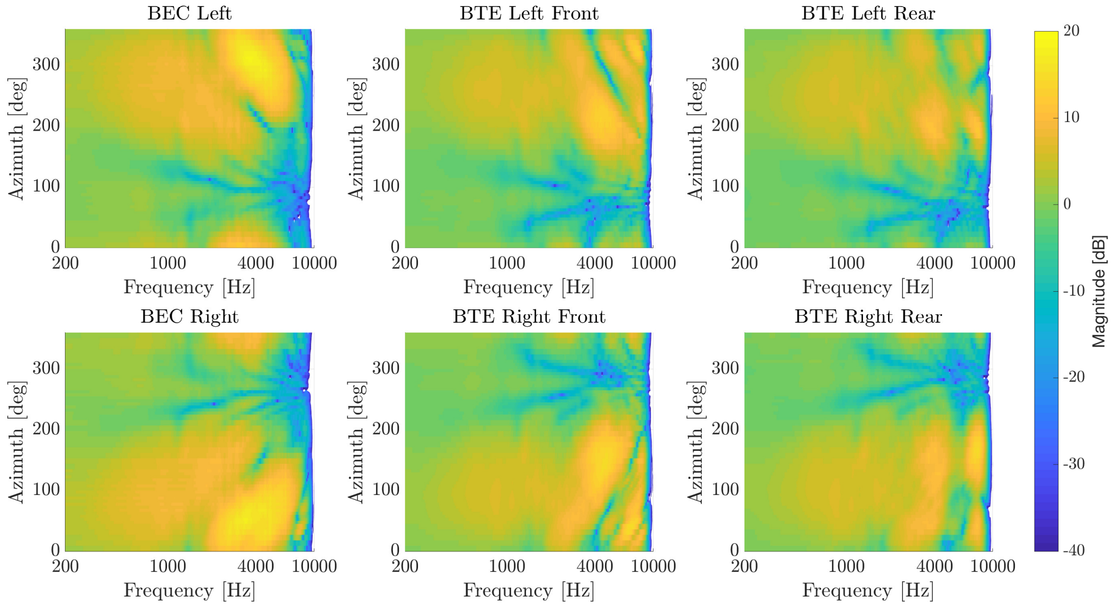

Figure A.5: Subject 1, $\varphi = -8°$

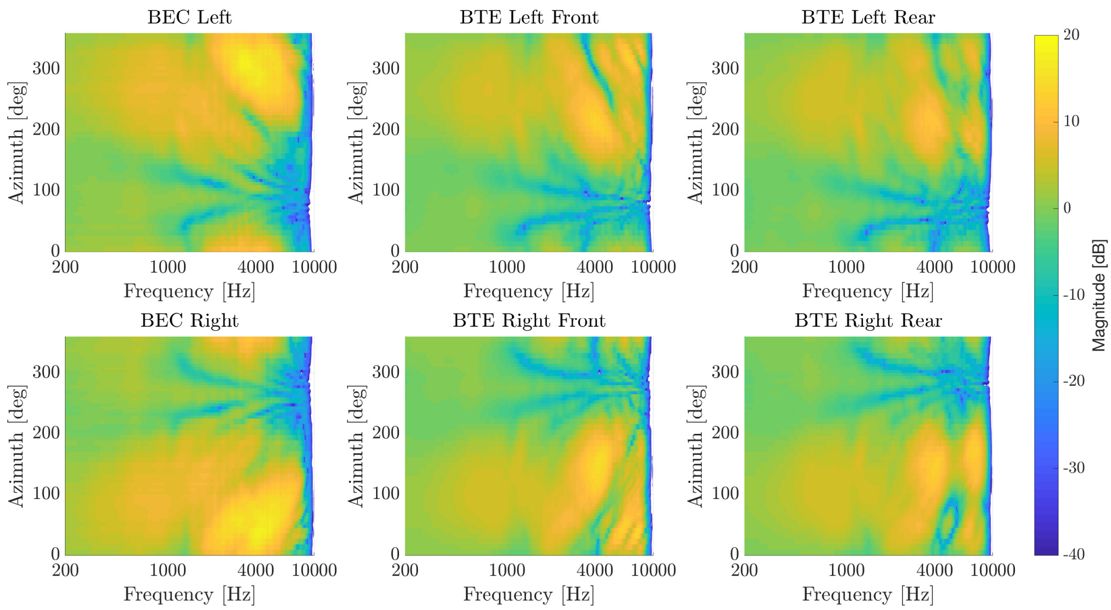

Figure A.6: Subject 1, $\varphi = 0°$

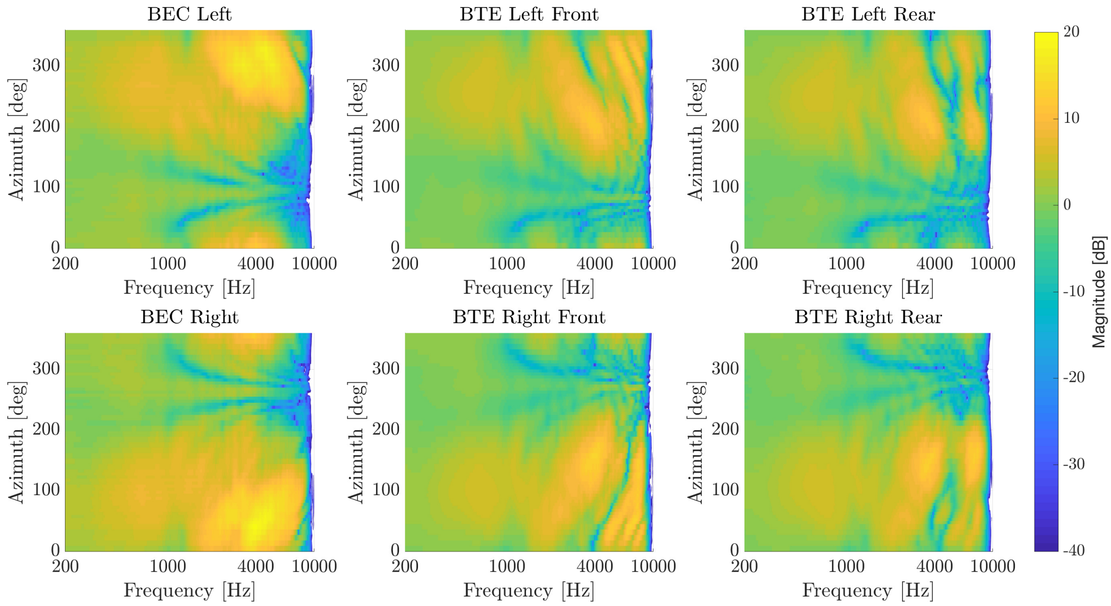

Figure A.7: Subject 1, $\varphi = 8°$

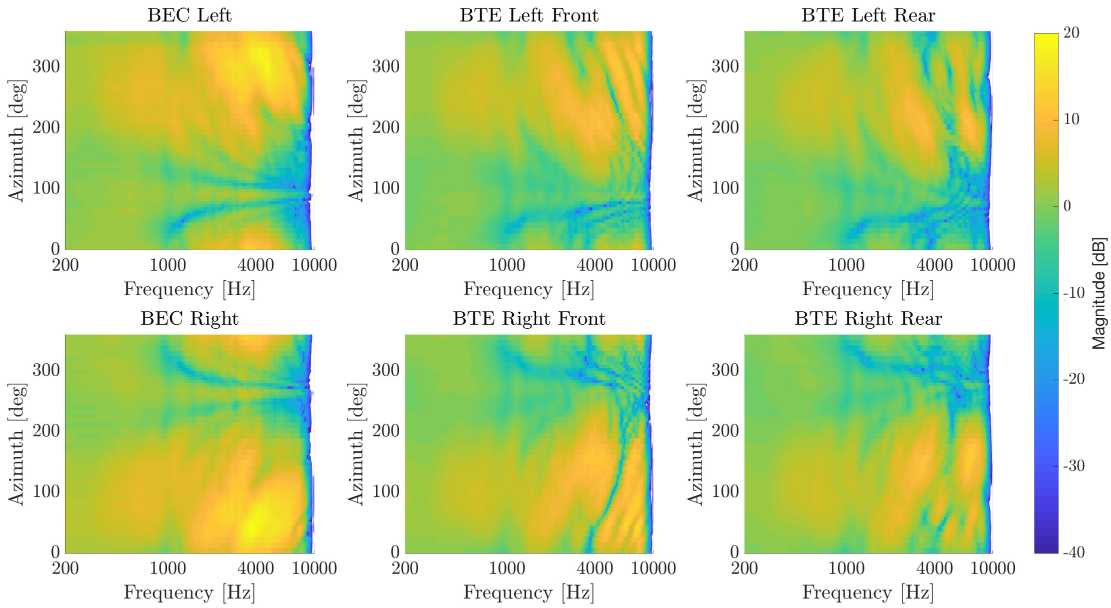

Figure A.8: Subject 1, $\varphi = 16°$

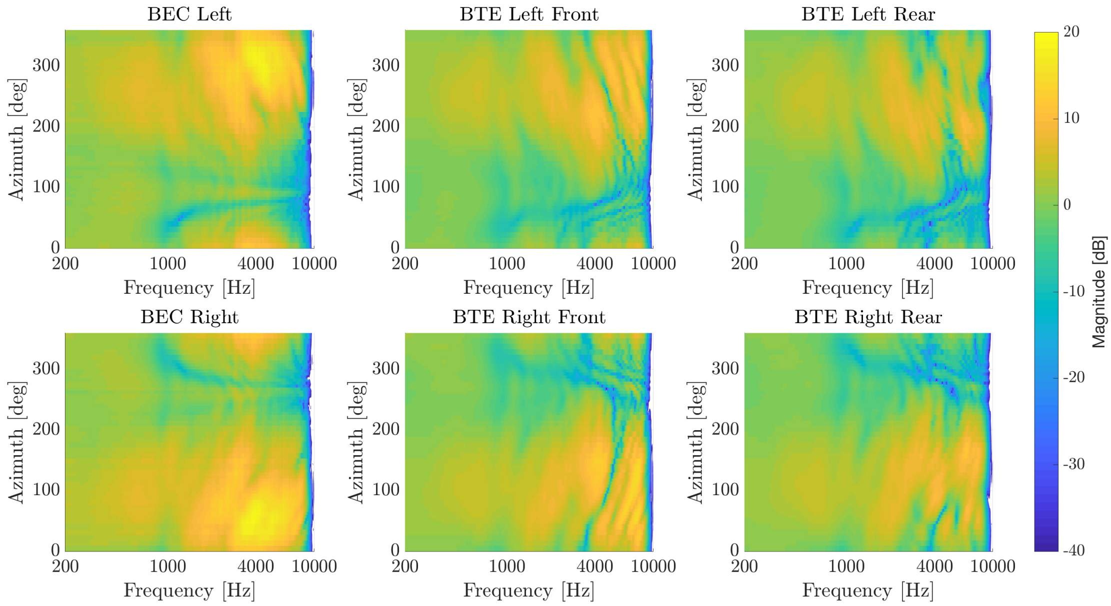

Figure A.9: Subject 1, $\varphi = 24°$

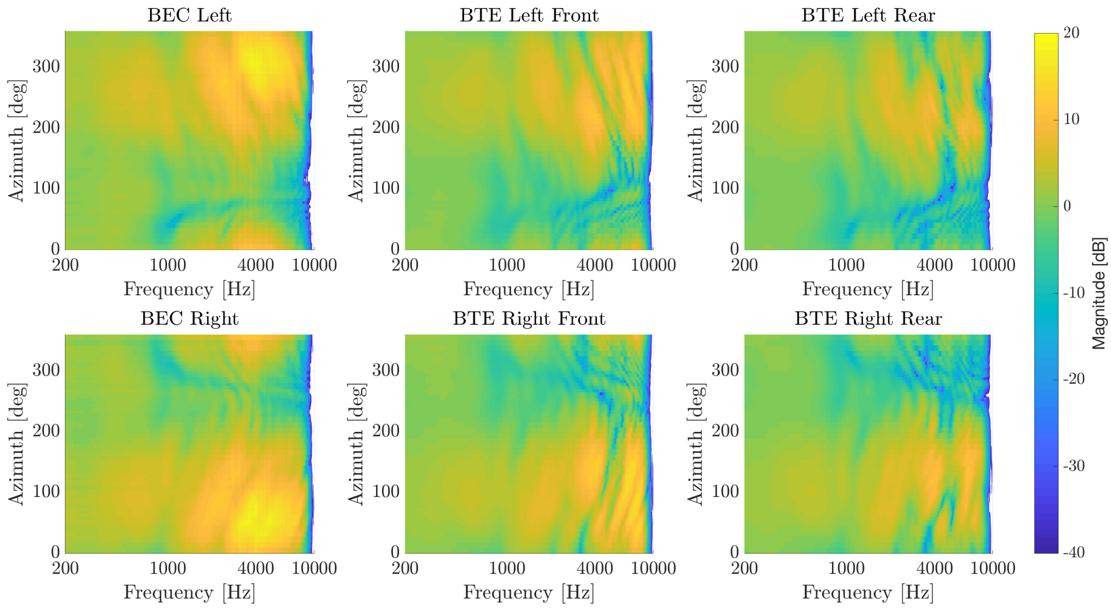

Figure A.10: Subject 1, $\varphi = 32°$

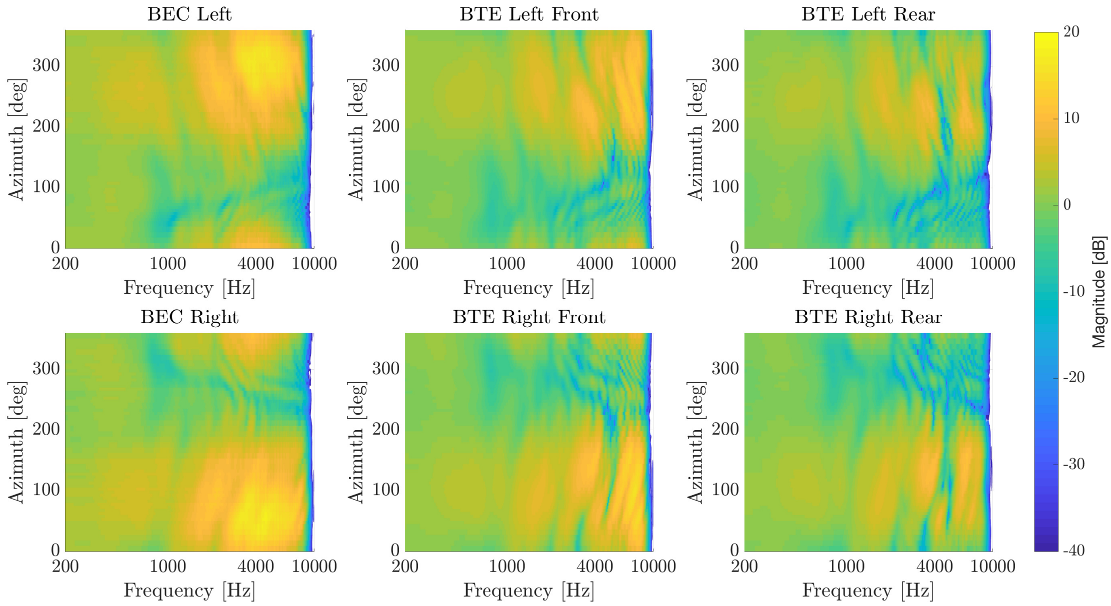

Figure A.11: Subject 1, $\varphi = 40°$

B | Digital Appendix

For the delivery of the thesis a digital appendix is delivered containing all HRTF plots for the 4 subjects measured similar to those found in Appendix A.

Each figures are named *HRTF_Subject_N_Speaker_X.eps* where X is an integer from 1 to 11 corresponding to elevation $\varphi = -40°$ to $40°$ in $8°$ increments and N being the subject index.

C | Pinna Reconstruction Transfer Functions

This appendix contains all HRTF plots for subject 1 for all 11 elevations measured. PRTF plots for all 4 subjects can be found digitally in Appendix D.

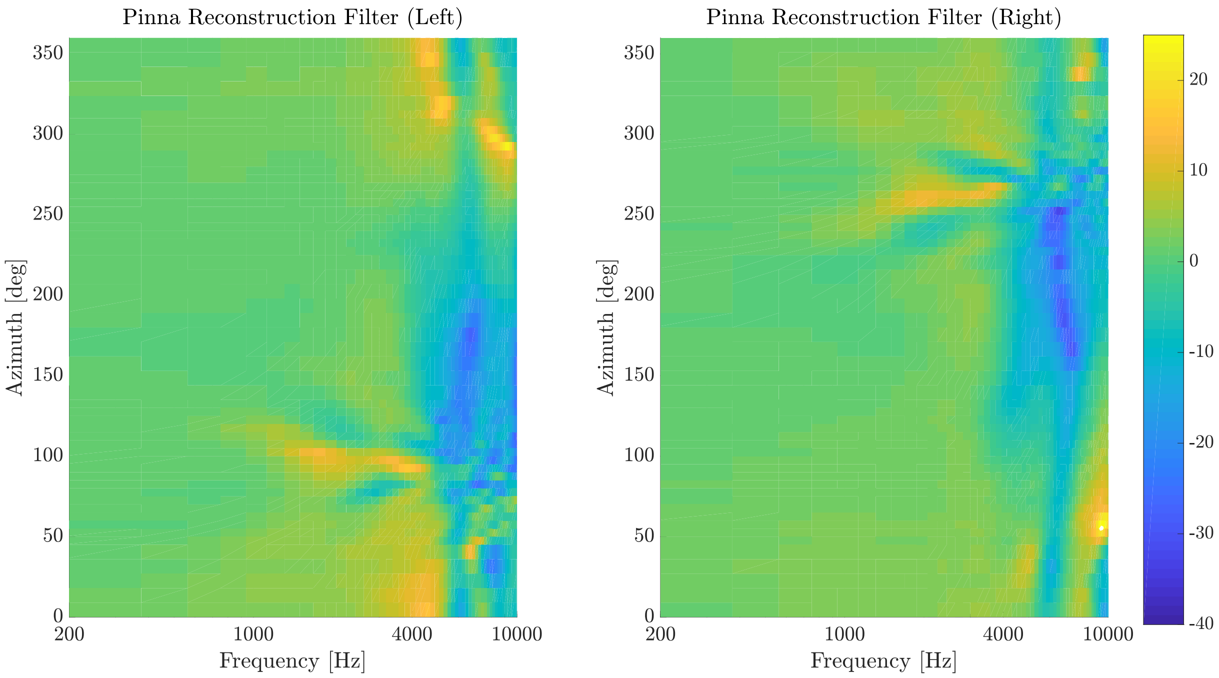

Figure C.1: Subject 1, $\varphi = -40°$

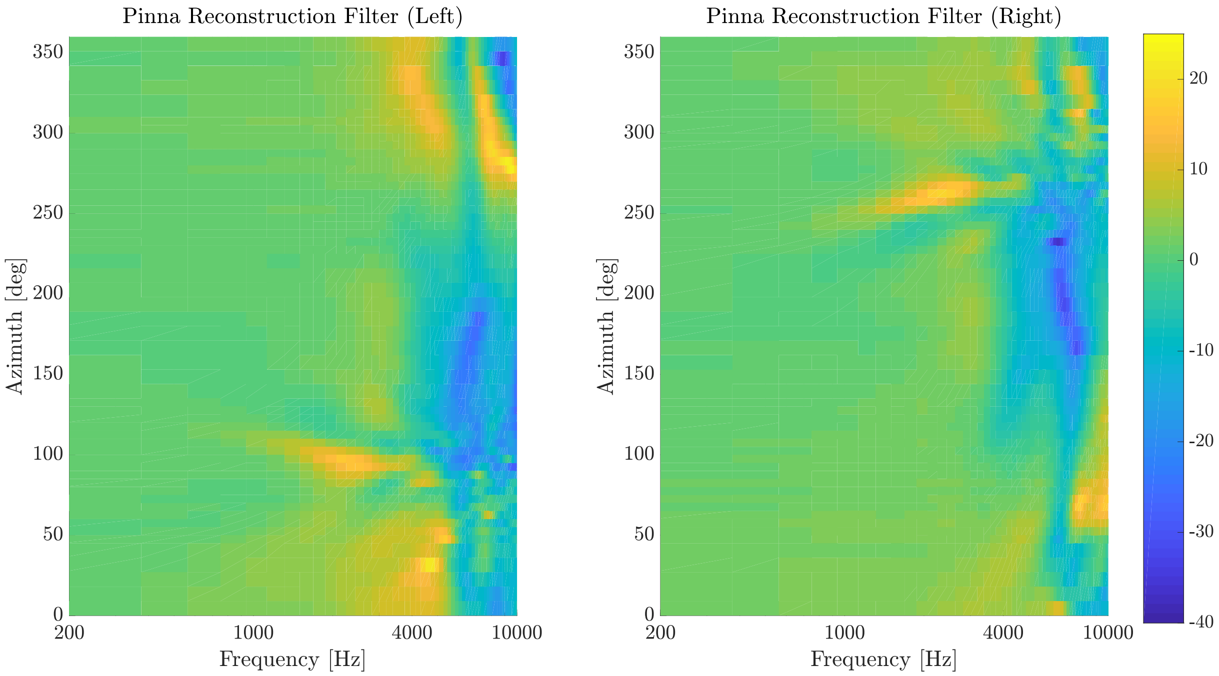

Figure C.2: Subject 1, $\varphi = -32°$

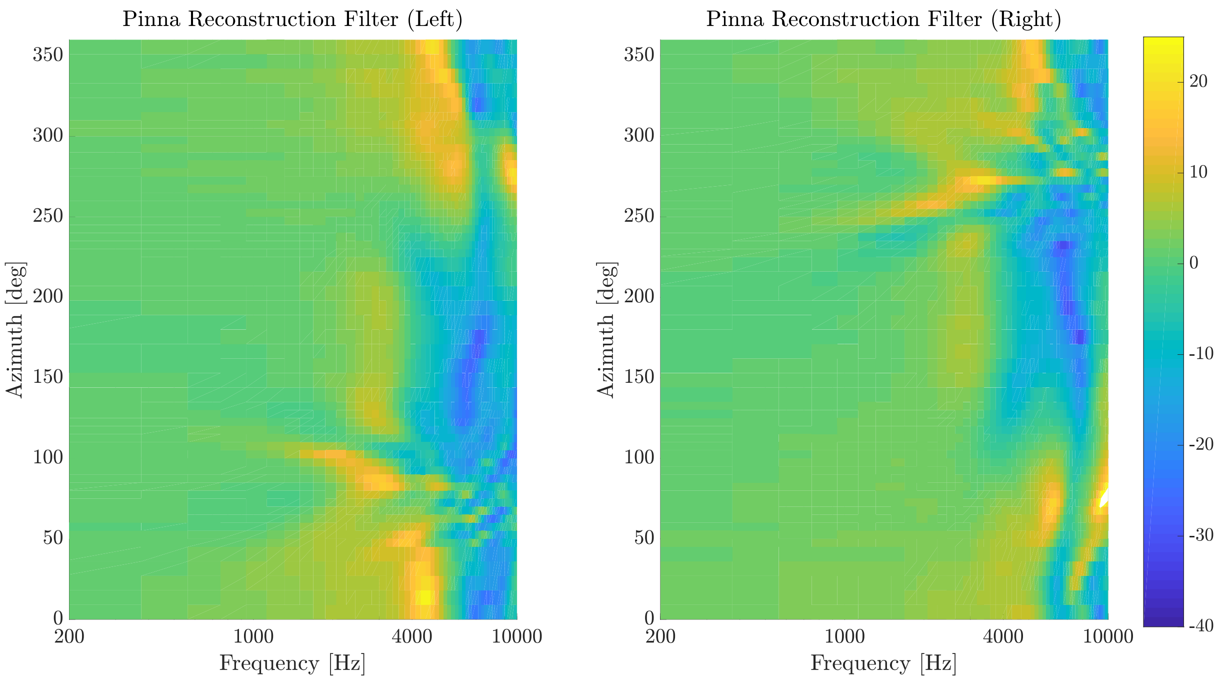

Figure C.3: Subject 1, $\varphi = -24°$

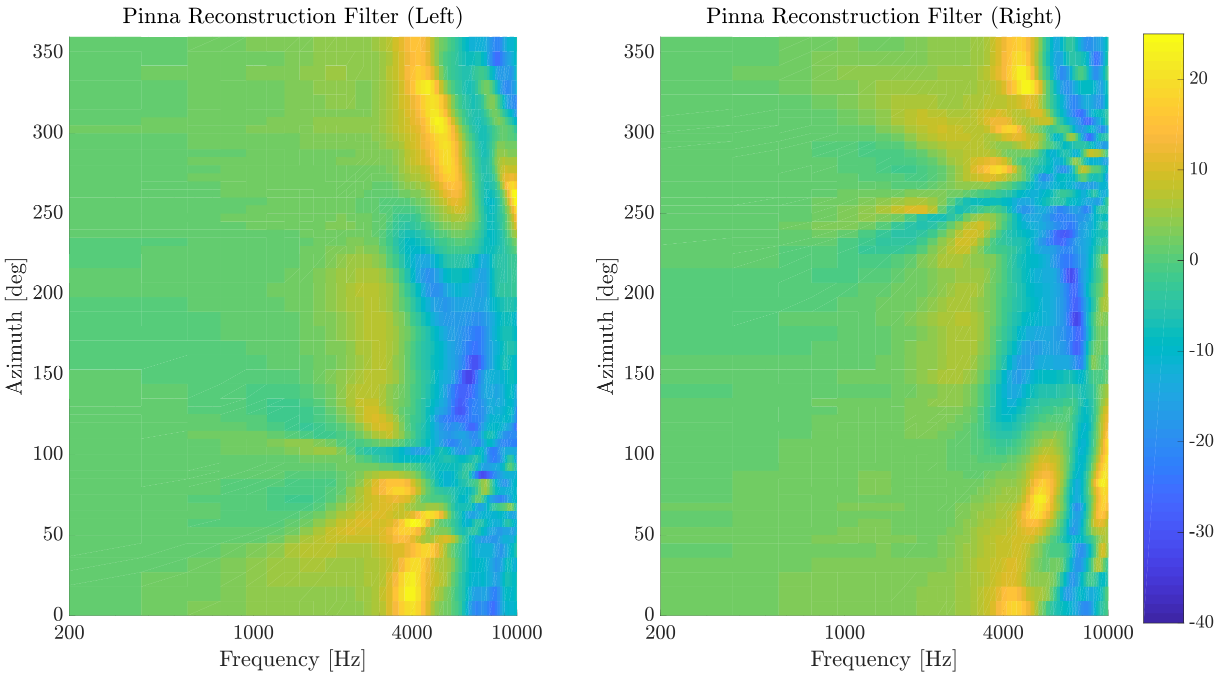

Figure C.4: Subject 1, $\varphi = -16°$

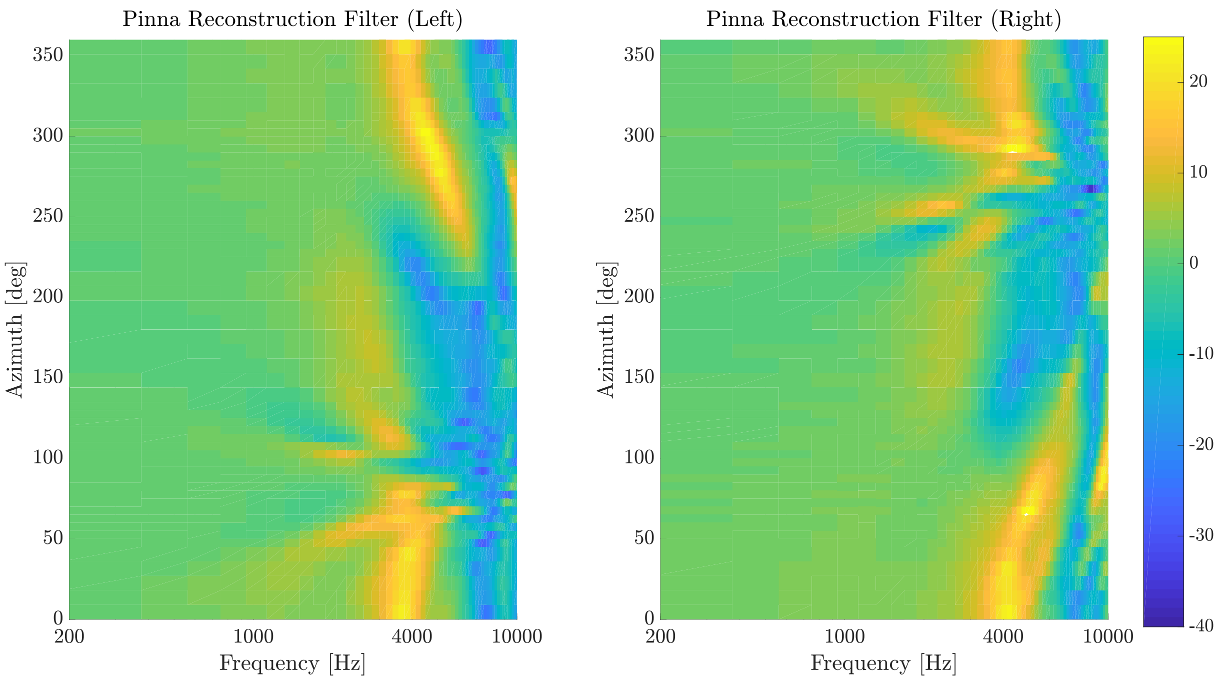

Figure C.5: Subject 1, $\varphi = -8°$

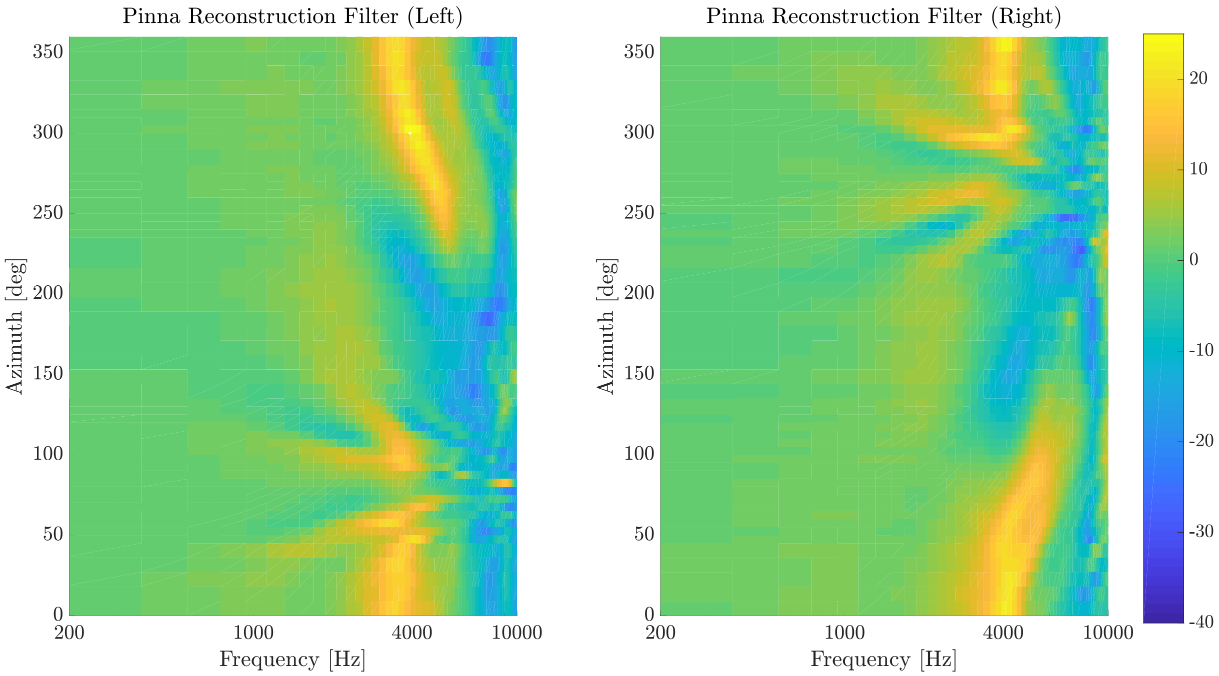

Figure C.6: Subject 1, $\varphi = 0°$

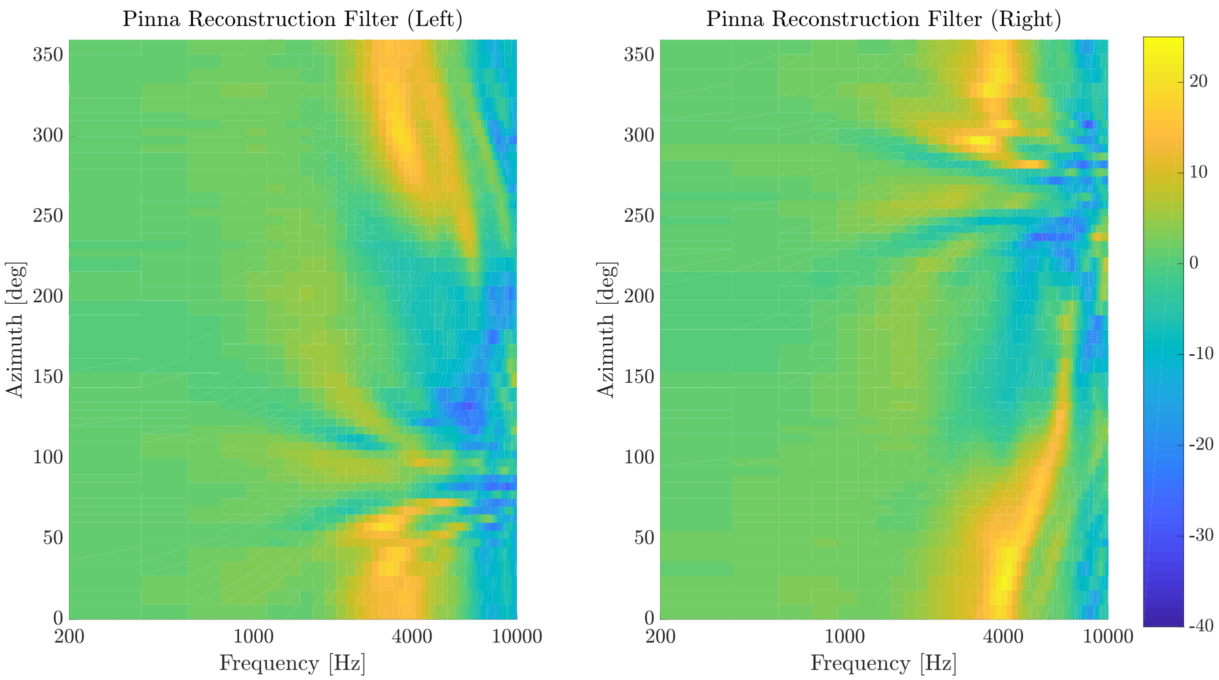

Figure C.7: Subject 1, $\varphi = 8°$

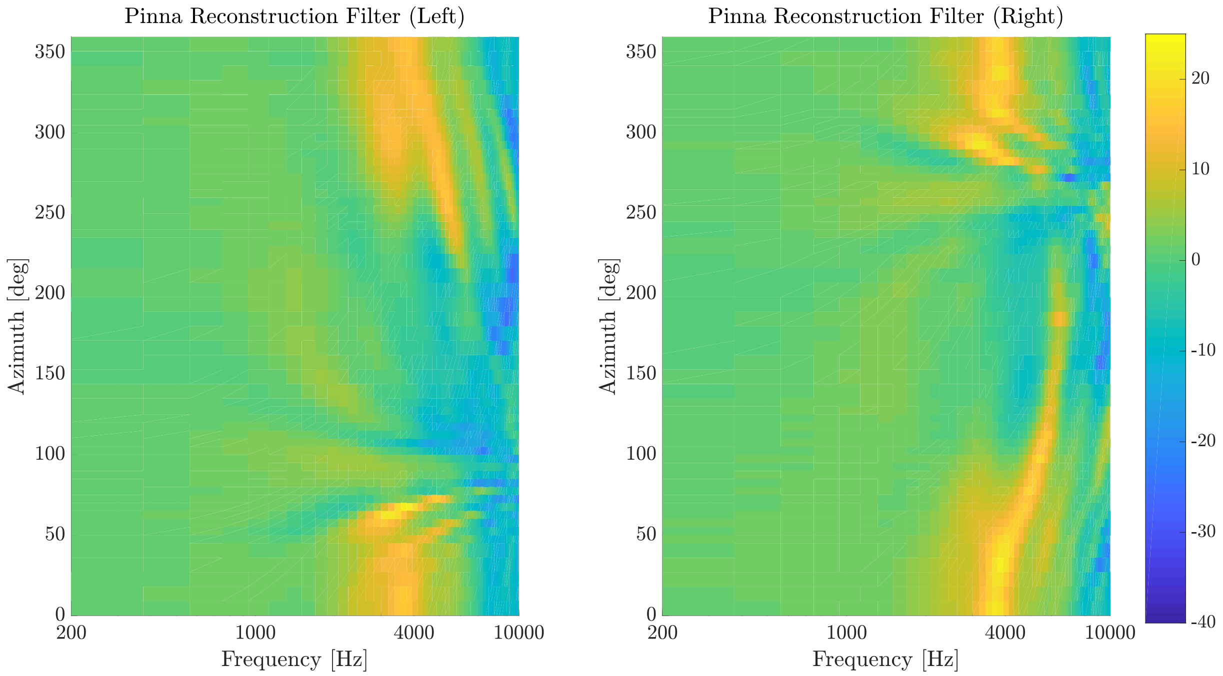

Figure C.8: Subject 1, $\varphi = 16°$

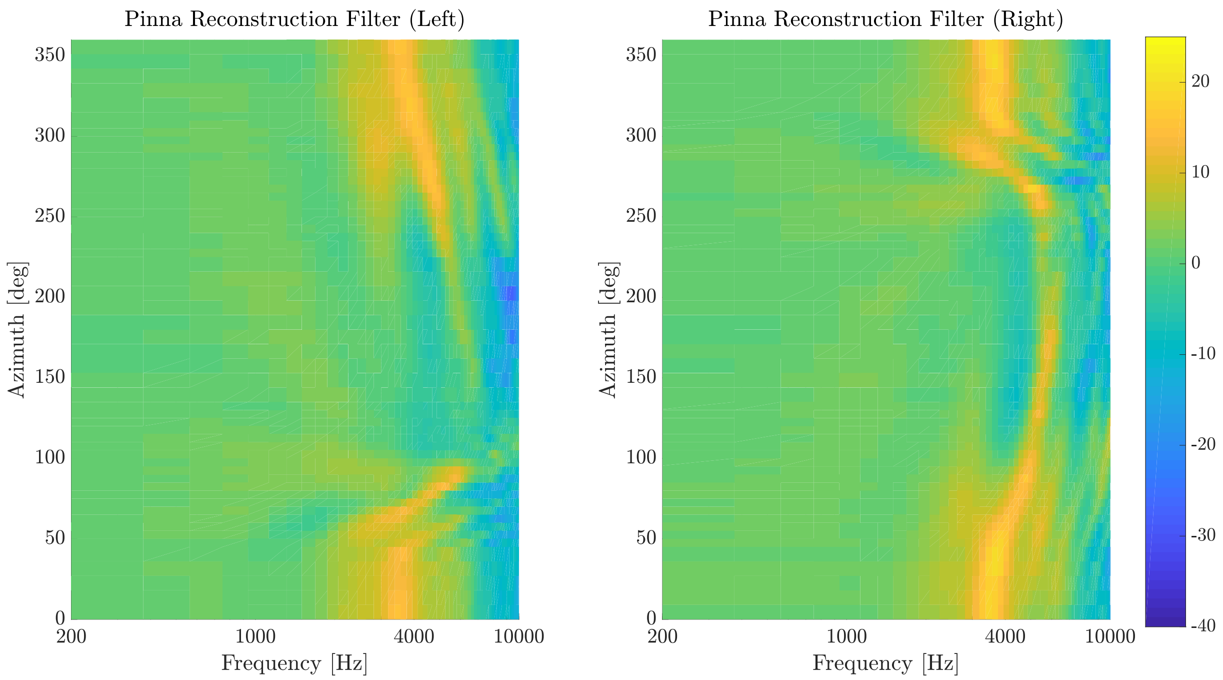

Figure C.9: Subject 1, $\varphi = 24°$

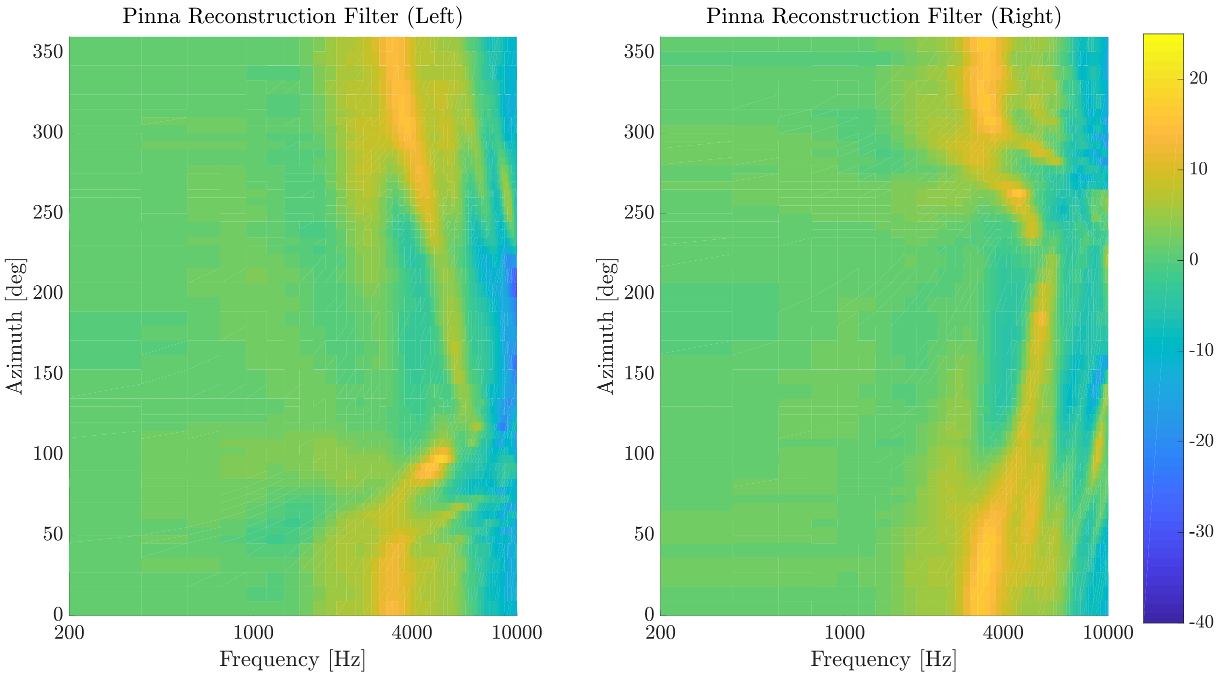

Figure C.10: Subject 1, $\varphi = 32°$

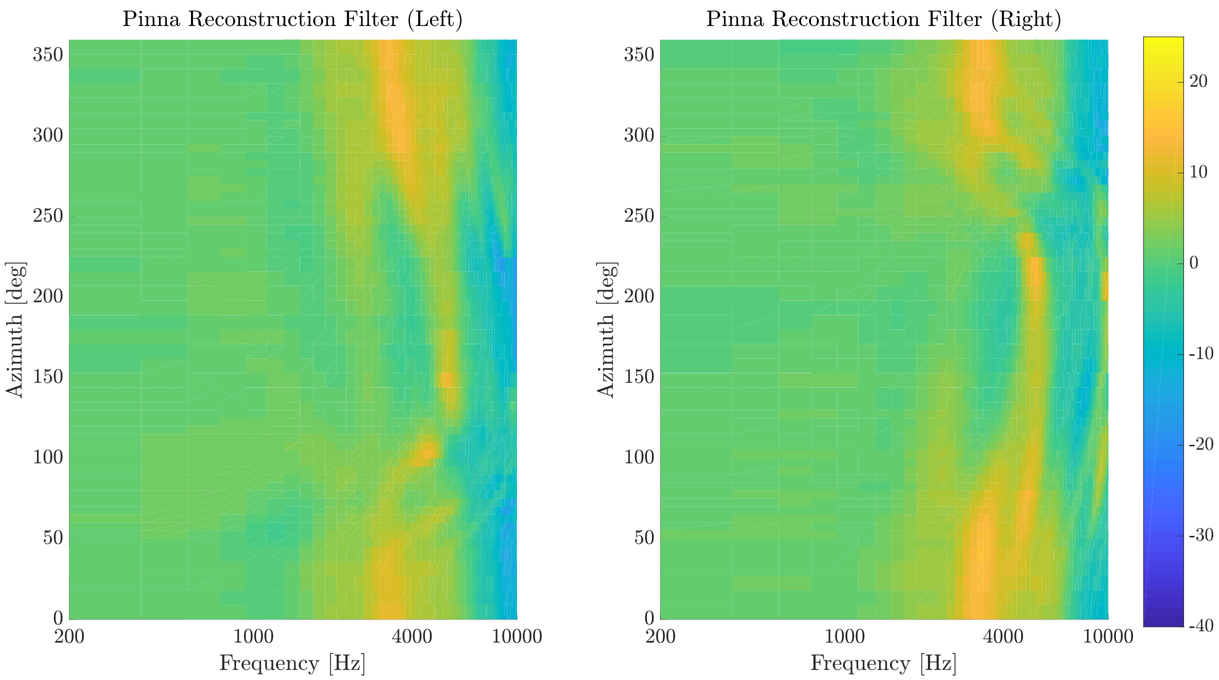

Figure C.11: Subject 1, $\varphi = 40°$

D | Digital Appendix

For the delivery of the thesis a digital appendix is delivered containing all PRTF plots for the 4 subjects measured similar to those found in Appendix C.

Each figures are named *PRF_Subject_N_Speaker_X.eps* where X is an integer from 1 to 11 corresponding to elevation $\varphi = -40°$ to $40°$ in $8°$ increments and N being the subject index.